

Development and Application of Quantitative Methodologies for the Characterization of Passive Hearing Protection Devices

Major Qualifying Project

Submitted to the Faculty of:
Worcester Polytechnic Institute

In Partial Fulfillment of the
Degree of Bachelor of Science

By

Sofia de Oliveira
Colleen Mullins
Jivan Purutyan
Lucas Reiniger
Brant Reymann

Date: May 18, 2020

Advisor: Professor Cosme Furlong



WPI



**Massachusetts
Eye and Ear**

Copyright © 2020

By Sofia de Oliveira, Colleen Mullins, Jivan Purutyan, Lucas Reiniger, and Brant Reymann

CHSLT – Center for Holographic Studies and Laser micro-mechaTronics

Mechanical Engineering Department

Worcester Polytechnic Institute

Worcester, MA 01609-2280

All rights reserved

Abstract

Hearing loss is a permanent condition that can greatly affect the quality of life. Protecting the auditory system subjected to different acoustical loads, including sustained noise and intense impulse sounds, is critical to minimizing the risks of impaired communication and of the limited physical abilities that can accompany hearing loss. Hearing protection devices are used to attenuate sound pressure levels at frequencies that would damage the sensitive organs of the ear. Passive hearing protection is the preferred method, as it relies on a combination of microstructure, material properties, and macro-scale geometries to attenuate sound pressure rather than using complex micro-electro-mechanical components of active hearing protection systems. In this project, we investigate the limitations of current passive hearing protection analytically, experimentally, and computationally to examine the relationships between microstructure, macrostructure, and performance. We developed and applied a testing apparatus and methods to isolate specific earplugs samples in order to assess their performance by measuring their corresponding Frequency Response Functions (FRFs) under sustained noise and high-intensity impulse blasts. The FRFs were analyzed and used to understand differences in attenuation between samples and to identify limitations in their acousto-mechanical design parameters. Concurrently, computational models were developed to parametrically investigate how microstructure, material properties, and earplug geometries attenuate different sound pressure levels and frequencies. It is expected that the combination of analytical, experimental, and computational results obtained in this project will enable future engineers to design and realize innovative passive hearing protection devices that incorporate advanced microstructures, geometries, and composite materials, together with advanced fabrication methods, in order to more effectively protect the human auditory system against different types of acoustical loads.

Keywords: Acoustic Attenuation, Frequency, Noise-Induced Hearing Loss, Passive Hearing Protection

Societal Implications

With Noise-Induced Hearing Loss as one of the leading causes of hearing loss, the development of proper hearing protection devices becomes more important every day. Hearing loss caused by damage to the internal organs of the middle and inner ear can greatly affect quality of life. With this methodology, earplugs can be developed that are specific to various frequencies present in a variety of fields, therefore reducing the exposure to damaging noises and improving the quality of life for millions of people around the world.

Acknowledgments

We would like to thank J.T. Cheng and John Rosowski from Massachusetts Eye and Ear for their feedback and insight over the past year. We would also like to thank our advisor, Professor Cosme Furlong, for his guidance and assistance throughout this project. Lastly, we would like to thank the WPI professors and faculty who have supported us in getting to where we are today.

We would also like to recognize the following individuals for assisting us and the success of our project:

Haimi Tang
Anthony Salerni
Daniel Ruiz-Cadalso

Authorship

All members contributed equally to this project.

Table of Contents

Abstract	2
Societal Implications	2
Acknowledgments	3
Authorship	3
Table of Contents	4
List of Figures	6
Objectives	9
1. Introduction	9
2. Background	11
2.1 <i>The Human Ear</i>	11
2.2 <i>Sound Waves</i>	12
2.2.1 Linear and Non-Linear Sound Waves	13
2.2.2 Sound Pressure	14
2.3 <i>Current Hearing Protection Devices on the Market</i>	15
2.3.1 Passive Hearing Protection	16
2.3.2 Current Testing of Passive Hearing Protection Devices	18
2.3.3 Material Properties of Hearing Protection Devices	19
2.4 <i>Overview of Past MQP</i>	22
3. Methodology	23
3.1 <i>The ANSI Standard</i>	23
3.2 <i>Experimental Setup</i>	24
3.2.1 Selection of Passive Hearing Protection	25
3.2.2 Testing Apparatus Development	26
3.2.3 Frequency Sweep Experiment	31
3.2.4 Anechoic Chamber Development and Verification	33
3.3 <i>Understanding the Microstructure and Macrostructure of Hearing Protection</i>	38
3.4 <i>Computational Model</i>	39
3.4.1 Purpose	40
3.4.2 Governing Equations	40
3.4.3 Porous Model Development	41

3.4.4 Triple Flange Model Development	43
4. Results	46
4.1 <i>Experimental Results</i>	46
4.1.1 Porous Earplugs	46
4.1.2 Non-Porous Earplugs	47
4.2 <i>Microscope Characterization of Microstructure and Shape</i>	49
4.3 <i>Computational Results</i>	52
4.3.1 Porous Earplug	52
4.3.2 Parametric Study	53
4.3.3 Triple Flange Earplug	56
5. Discussion	57
5.1 <i>Microstructure, Macrostructure, and Performance</i>	57
5.2 <i>Developing the Correlation</i>	58
5.3 <i>Application to Additive Manufacturing</i>	60
6. Conclusions and Recommendations	60
6.1 <i>Difficulties Driven by COVID-19</i>	61
7. Future Work	61
7.1 <i>Apply to a Nonlinear System: Shock Tube</i>	61
7.2 <i>High-Speed Imaging</i>	62
7.3 <i>Using Computational Model to Make Design Recommendations</i>	63
References	64
Appendices	67
<i>Appendix A: Safety Protocol</i>	67
<i>Appendix B: Frequency Sweep Operating Procedure</i>	68
<i>Appendix C: LabVIEW Code for Frequency Sweep Experiment</i>	69
<i>Appendix D: Frequency Sweep Experimental Setup Diagrams</i>	72
<i>Appendix E: Porosity Calculations</i>	74
<i>Appendix F: Microscopy Results for Various Sample Cross-Sections</i>	77
<i>Appendix G: Detailed Computational Setup</i>	80
<i>Appendix H: Instructions to Develop Computational Model</i>	87
<i>Appendix I: LabView Code for Shock Tube</i>	91

List of Figures

Figure 1: Diagram of the Human Ear That Shows the Internal Bones and Components that Allow for Hearing [4]	11
Figure 2: Diagram of the Compression and Expansion Components of a Longitudinal Sound Wave [9]. Sound Waves Travel at the Speed of Sound Modulated by the Source	12
Figure 3: Diagram of the Frequency Response Function System. An input	14
Figure 4: Schematic of Electronic System Active Protection	16
Figure 5: Examples of Various Triple Flange Earplugs Currently on the Market [23]	17
Figure 6: Examples of Various Level-Dependent Earplugs Currently on the Market [23]	17
Figure 7: Examples of Foam Earplugs Currently on the Market [23]	17
Figure 8: Examples of Banded Hearing Protection	17
Figure 9: Energy Loss Stress-Strain Curve [28]	20
Figure 10: Damping Coefficient [28]	20
Figure 11: Experimental and Computational Results Obtained with a Shock Tube [29].	22
Figure 12: Drawing for ANSI S12.6 Pinna Fixture [30].	24
Figure 13: Passive Hearing Protection Samples.	25
Figure 14: SolidWorks Model of ANSI S12.6 Pinna Fixture: Isometric View, Side View.	26
Figure 15: Pinna Fixture Precision Manufactured and	27
Figure 16: Platform and Tracks Used in the Experimental Setup that Allowed for Adjustable Distance and Height.	28
Figure 17: Pinna Fixture on Adjustable Platform with Sound Blocking Barrier, Custom Manufactured Mounting Plate, and Speaker	29
Figure 18: Sound Barrier Manufactured for Experimental Setup, 1 ft by 1 ft.	30

Figure 19: Complete Experimental Setup With Anechoic Chamber, Sound Absorbing Foam, Microphones, Sound Blocking Barrier and Speaker	31
Figure 20: LabVIEW Block Diagram FRF Function	32
Figure 21: LabVIEW for Sweep Experiment Front Panel.	33
Figure 22: CAD Model of Pinna Fixture Used in COMSOL to	34
Figure 23: COMSOL Model of the Pinna Fixture With Inserted Earplug	34
Figure 24: CAD Model of the Sound Barrier Used in COMSOL	35
Figure 25: Completed Model of Enclosure, Sound Blocking Barrier,	36
Figure 26: Four Different Enclosure Geometries Tested for Accuracy of	36
Figure 27: Pressure Distribution within Simulated Enclosure with Point	37
Figure 28: Convergence Plot Showing Effect of Enclosure Size on Earplug	38
Figure 29: Sample 1 Observed Under 100x Magnification.	39
Figure 30: Computational Model in the Context of the Ear	41
Figure 31: Computational Model of Porous Earplug. Earplug, Shown in Yellow, Based off Reference Geometry.	41
Figure 32: Porous Earplug Multiphysics Domains.	42
Figure 33: Porous Earplug Boundary Conditions. Earplug Fully	43
Figure 34: Triple Flange Computational Setup.	44
Figure 35: Triple Flange Boundary Conditions. Uniform Pressure Front of 1 Pa	45
Figure 36: Triple Flange Material Domains. Earplug (shown in blue) Modeled	45
Figure 37: Porous Earplug Samples Used for Testing. Chosen Because of Differing	46
Figure 38: Porous Earplug FRF Comparison.	47
Figure 39: Representative Geometry of Triple Flange Earplug	48

Figure 40: Moldable Silicone Putty Earplug with Demonstration of	48
Figure 41: FRF Comparison of Non-Porous Earplugs.	49
Figure 42: Sample 1 Observed Under 100x Magnification. 3D Elevation, Greyscale Image	50
Figure 43: Porous Earplug Model in COMSOL Based on Reference Plug Geometry.	52
Figure 44: Sound Pressure Level Distribution in Computational Geometry at 1 kHz.	53
Figure 45: Results of Porosity Parametric Study	54
Figure 46: Results of Viscous Length Parametric Study	55
Figure 47: Results of Fluid Matrix Density Parametric Study	56
Figure 48: Cross-sectional Triple Flange Pressure Distribution.	57
Figure 49: Our Process Considered Microstructure along with Macro Structure to Understand the Effect on Overall Attenuation	58
Figure 50: Microstructure and Performance Between Porous and Non-Porous Samples.	59
Figure 51: Diagram of Experimental Setup Viewed from the Output of the Shock	62
Figure 52: Diagram of Aerial View of Experimental Setup Including the High-Speed Camera and Mirror Used for Schlieren Imaging.	62
Figure 53: Image Captured Using the High-Speed Camera and Schlieren Technique.	63

Objectives

The objective of our project is to understand the relationships between microstructure, macrostructure, and material properties on the performance of passive hearing protection in order to improve current designs. We plan to achieve this by completing the following objectives:

1. Understand sound waves, both linear and nonlinear, and sound wave attenuation.
2. Develop an adjustable experimental setup that allows for the testing of a variety of samples with different stimuli to observe how sound waves are attenuated.
3. Develop a computational model to understand the effect of varying material properties on attenuation.
4. Develop a computational model to understand the effect of varying macrostructure (geometry) on attenuation.
5. Utilize a high magnification microscope with data collection abilities to observe the microstructure of earplug samples and draw a link between microstructure and attenuation.

1. Introduction

Hearing loss is a problem that millions of people around the world suffer from. In the United States specifically, 15% of adults (people over the age of 18 years old) have reported that they experience some form of hearing impairment. Hearing loss can be a result of a variety of different factors including genetic diseases, old age, physical head trauma, and exposure to loud noises. At least 10 million adults are experiencing some form of hearing loss, yet as many as 40 million adults have had hearing tests that indicate that they have hearing loss in one or both ears from exposure to loud noise. This is called Noise-Induced Hearing Loss (NIHL). NIHL is a direct result of exposure to loud noises. If the exposure is short but intense, the sound needs to be around 100 dB SPLs to cause damage. If the exposure is over a long period of time, then the sound need only be at a low decibel of 85 to cause NIHL. Some of these loud noises that people are exposed to are from everyday items and activities, including target shooting, listening to music at high volume, and mowing the lawn [1].

Although there are current hearing protection devices on the market that are supposed to prevent NIHL, it is still a very prevalent issue, with millions of Americans afflicted. The most common current hearing protection devices on the market include earplugs and earmuffs which attempt to effectively attenuate high intensity sounds and mitigate hearing loss. Within these two product categories, they can be divided further into active hearing protection and passive hearing protection. Active hearing protection can be two earplugs or an earmuff headset that contains a

digital audio signal processing unit that is connected to an audio input and output. Passive hearing protection mitigates noise exposure and prevents hearing loss by attenuating sound waves and preventing damaging noises from entering the ear canal.

Our project will focus on the dampening characteristics of passive hearing protection. The most common types of passive hearing protection are earmuffs and earplugs. Unlike active hearing protection, passive protection relies on the material and physical structure to dampen sound. The microstructure of the earplug material, along with the physical design of the earplugs, combine to give passive hearing protection its dampening characteristics. There are several different styles of passive hearing protection including custom molded, shaped, and expandable [2]. The custom-molded protection is typically made with a putty-like material, such as silicone, that is made to mold to each user's ear canal. The damping characteristics of this type of material is dependent on how well the user molds it to their ear. Pre-molded earplugs can be made from soft, solid plastic. However, the material is not the main source of damping, its unique "flanged" shape does most of the damping. The last and most common style of earplug is categorized as expandable. These earplugs are cylindrical in shape, sometimes tapered at the end, and made from a soft, porous foam such as polyurethane. These are known to be the most comfortable because the foam is compressed before placing it into the ear canal and slowly expands to fit the canal. The snug fit and porous material are responsible for its damping characteristics.

The current products on the market, although may dampen sound, are still allowing damaging frequencies to pass into the ear. Currently, earplugs are being tested for how well they attenuate frequencies after manufacturing. There is a gap in the design process to test the effectiveness of earplugs prior to being made, specifically for selective frequency damping (i.e. choosing which specific frequencies will not be allowed to pass through the passive hearing protection). In order to close this gap, there needs to be a better understanding of how the linear and non-linear attenuation of hearing protection devices affects the relative dampening of high-intensity sounds vs. low-intensity sounds.

To prevent future hearing loss, testing methods, and computational analyses were developed for both linear and non-linear regimes to understand how microstructure, macrostructure, and material properties can impact the performance of the earplugs. With this information, and by investigating the linear and non-linear attenuation of sound waves through passive hearing protection devices, this project aims to relate the microstructure, macrostructure, and/or material properties of an earplug to its transmissivity in order to make recommendations for creating an effective earplug.

2. Background

2.1 The Human Ear

The human ear is split into three parts: the outer ear, the middle ear, and the inner ear. Each part of the ear plays an important role in the hearing process. Sound waves travel through the outer ear and are directed to the middle ear by the pinna. The middle ear is comprised of the tympanic membrane, also known as the eardrum, and three small bones: malleus, incus, and stapes. Once the sound waves reach the middle ear, the tympanic membrane (TM) vibrates the sound waves through to the three bones. Each of the three bones amplifies the sound waves and sends them to the inner ear. In the inner ear is the cochlea, a snail shell-shaped bone that is filled with potassium-rich fluid. The sound waves' vibrations cause the fluid to ripple and make waves through the cochlea causing the hair cells to bend [3]. When the hair cells bend, ion channels open and potassium ions enter the channel creating an electric signal which is carried to the brain to be interpreted by the auditory nerve [3]. A diagram of the human ear can be seen in Fig. 1 detailing the various components critical for hearing.

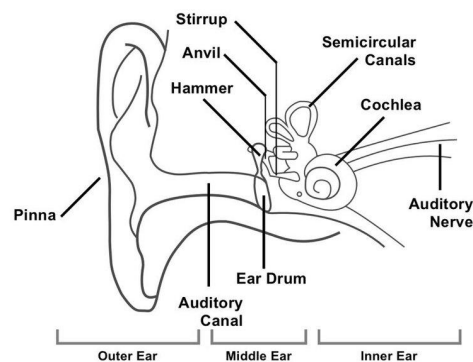


Figure 1: Diagram of the Human Ear That Shows the Internal Bones and Components that Allow for Hearing [4]

A potential cause of hearing loss is damage to the cochlea's hair cells. The cochlea has 15,500 hair cells at birth, 12,000 outer and 3,500 inner, which cannot regrow. Damage to these hair cells can be caused by overstimulation [5]. The beginning of the cochlea is responsible for receiving high-frequency sounds [5]. Since high-frequency noises are known to cause damage or death to these hair cells, exposure to loud noises for long periods of time should be minimized [5]. Therefore, eliminating long exposure to general noises, or any exposure to loud noises will have a positive effect on the hearing.

The ear protects itself from loud noises through a reflex called the acoustic stapedius reflex (ASR). This happens with the stapedius muscle contracts within one-tenth of a second after being exposed to loud noise [6]. The sound of your own voice, a cough, or a sneeze can trigger the ASR which allows the ear to protect itself. Once the stimulus has been heard, the stapedius and tensor tympani muscles in the ear contract [7]. The stapedius muscle pulls down on the stapes, which is found in the middle ear, away from the oval window of the inner ear which stiffens the ossicular chain. In tandem, the tensor tympani muscles stiffen the ossicular chain by pulling the malleus toward the middle ear which loads the tympanic membrane. The contraction of these two muscles stiffens the middle ear which prevents it from amplifying sound to the inner ear in turn protecting the cochlea.

While the ear can protect itself, its own mechanisms are not always enough. Simple everyday tasks, such as vacuuming, can cause damage to ears. This develops a need for hearing protection devices. As mentioned previously, there are two different types of hearing protection, active and passive. Active hearing protection requires an electronic system to dampen sound waves, while passive hearing protection relies on material and shape. The simplicity of passive hearing protection, and a device that dampens frequencies of interest, is much needed.

2.2 Sound Waves

Sound waves are produced by a vibrating body. The vibrations of this body cause the particles in the medium surrounding it to also vibrate. This vibration of the medium creates longitudinal waves [8]. Sound waves have sections of compression (high pressure) and rarefaction (low pressure). The distance from one compression or rarefaction to the next adjacent compression or rarefaction is the wavelength of a sound wave [5]. The amplitude of the sound wave can be characterized by the measure of high pressure in the compressed section of the longitudinal wave. A diagram of the components in a longitudinal sound wave can be seen in Fig. 2.

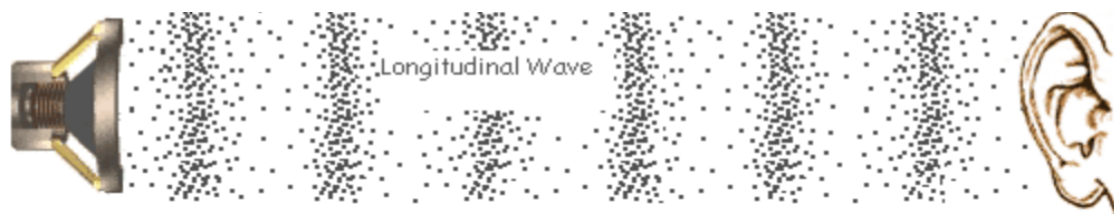


Figure 2: Diagram of the Compression and Expansion Components of a Longitudinal Sound Wave [9]. Sound Waves Travel at the Speed of Sound Modulated by the Source

There are different ways an ear can be subjected to acoustics. The first and simplest kind is known as a tone. A tone is a sound whose amplitude changes as a sinusoidal function of time [10]. These simple tones only have one frequency that represents a sine wave. There is a stimulus known as a chirp, which is a sweep through the desired set of single tone frequencies. Another way ears are subjected to acoustics is through a shock wave or a blast. A conical shaped area of pressure waves is created when the speed of a source is greater than the speed of sound. The edge of the cone forms a supersonic wave front of unusually high amplitude which is called a shock wave. Once this wave reaches an observer, a boom is heard. These shocks can be created in blast tubes, which are similar to micro explosives.

2.2.1 Linear and Non-Linear Sound Waves

All sound waves can be modeled by partial differential equations. Differential equations are equations with independent variables, an unknown function, and the partial derivative of that unknown function [11]. The number and type of equations used to model a sound wave determine if they are linear or nonlinear. Linear sound waves are described by linear equations and can be found by a combination of simple explanations. Non-linear sound waves are described by non-linear equations which makes them more complicated as each aspect of the wave needs to be treated as an individual wave. The equation for the intensity of nonlinear sound waves is described by Eq. 1 where I is the intensity, ρ is the density of the medium the sound is traveling through, δ is the amplitude of the sound wave, c is the speed of sound, and ν is the frequency of the sound [12],

$$I = 2\pi^2\rho\delta^22cv. \tag{1}$$

Another difference between linear and nonlinear waves is if the superposition principle can be applied. The superposition principle says that sound waves can be at the same place in space at the same time and not disturb each other [13]. For example, if two people were talking at the same time, the sound waves created from each person can coexist in the space between them. The superposition principle can only be applied to linear sound waves. Nonlinear sound waves cannot coexist in the same space; therefore, the superposition principle does not apply.

Linear and non-linear waves have different responses to stimuli as well. As described in this paper, linear waves show no signs of ringing, while nonlinear waves induce ringing. Ringing is the “strong transient response that decays to steady-state at a rate that depends on the system that is damping” [14]. The best way to identify how well a physical system is damping is through a frequency response function, however, they can only be applied to linear systems. A frequency response function (FRF) is the relationship between the output and input of a system [15]. An

FRF is a function in the frequency domain that is produced when the output of the system is divided by the input. These functions are used to show the attenuation of the system at a range of frequencies. For example, an FRF value of 1 signifies that no sound was attenuated and a value of 0 signifies all sound was attenuated. A visual explanation of a Frequency Response Function is shown in Fig. 3.

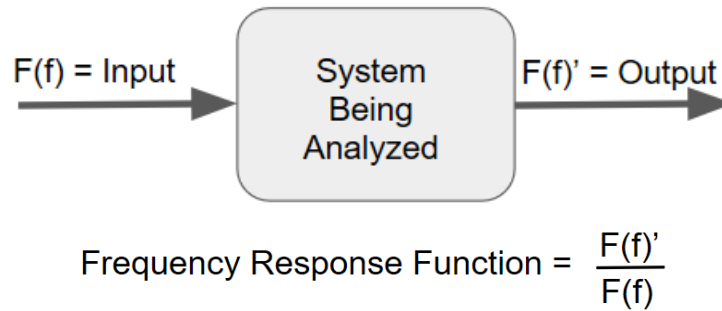


Figure 3: Diagram of the Frequency Response Function System. An input function is sent into a system and transformed. From this transformation, the new function, known as the output function, created by this transformation is developed and can be seen leaving the system. To find the Frequency Response Function of a system, divide the output by the input

2.2.2 Sound Pressure

Sound waves are sometimes referred to as pressure waves due to their sections of high and low pressure. As mentioned above, the high and low-pressure areas are known as compressions and rarefactions, respectively. The more pressure that a compressed section of a wave holds will create a louder sound level [8]. This sound level (or pressure) is measured in decibels (dB SPL). Decibels are measured on a logarithmic scale to better compare the extremely large range of sounds that the human ear can register. To give some reference to dB SPL measurements, Table 1 shows everyday noises and their corresponding sound pressure levels.

Table 1: Sound Pressure Levels of Everyday Noises [16]

Everyday Sounds and Noises	Average Sound Level in dB SPL
Normal Breathing	10
Soft Whisper	30
Washing Machine	70
City Traffic	80 - 85
Motorcycle	95
Approaching Subway Train	100
Firecrackers	140 - 150

Equation 2 can be used to calculate the sound pressure level, where P is the measured sound pressure, and P_0 is the reference sound pressure, or the quietest sound audible by the human ear [5]. The equation for sound pressure level is,

$$L_p = 20 * \log\left(\frac{P}{P_0}\right) . \quad (2)$$

There are three ways to quantify the pressure in a sound wave: static pressure, dynamic pressure, and stagnation pressure. Static pressure is the pressure of the wave in reference to atmospheric pressure. Dynamic pressure is the pressure associated with the kinetic energy of the wave. Lastly, the stagnation pressure is the pressure felt when the moving fluid is brought to rest [17]. Equation 3 can be used to relate these three measurements:

$$P_{\text{stagnation}} = P_{\text{static}} + P_{\text{dynamic}} . \quad (3)$$

2.3 Current Hearing Protection Devices on the Market

Hearing enables individuals to connect to the world for many, vital reasons [18]. Unfortunately, hearing loss can impact these actions, particularly in military and law enforcement situations. Military and law enforcement personnel are the most at risk for hearing loss due to frequent exposure to high-intensity sounds. The prevalence of hearing loss among military personnel is high, present in roughly 30% of employees, three times the prevalence in the general population

[19]. This data reassures the need for high-quality hearing protection devices. The most common hearing protection devices to effectively attenuate high intensity sounds and mitigate hearing loss are earplugs and earmuffs [20]. Among these two products, they both can be categorized further into active hearing protection and passive hearing protection. Active hearing protection can be two earplugs or an earmuff headset that contains a digital audio signal processing unit which is connected to an audio feedback control [21]. A diagram of an active hearing protection device is shown in Fig. 4.

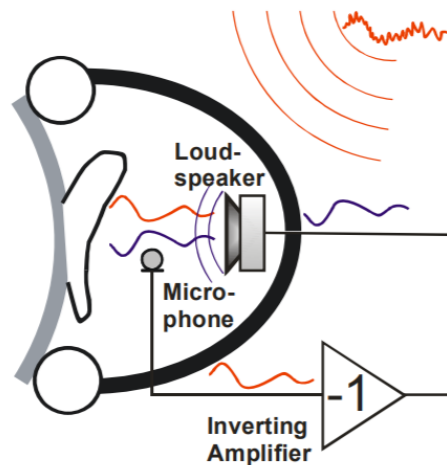


Figure 4: Schematic of Electronic System Active Protection Utilizes to Attenuate Sound [21]

The microphone is capable of detecting sounds coming into the headset and determining if the sound is harmful or not. The microphone signal will then be processed by the controller [22]. If the signal is determined to be harmful, the speaker outputs a sound in the ear canal. The microphone continues to measure the noise by the ear canal and makes adjustments as needed. Another benefit of active systems is that they can enhance low noises at the conversational level, but they are often heavier and more costly.

2.3.1 Passive Hearing Protection

Our project will focus on the dampening characteristics of passive hearing protection. Passive hearing protection mitigates noise exposure and prevents hearing loss by attenuating sound waves and preventing damaging noises from entering the ear canal. The most common types of passive hearing protection are earmuffs and earplugs. Unlike active hearing protection, passive protection relies on the material structure and overall shape to dampen sound. The internal pore structure of the actual material along with the macrostructure design of the earplugs combine to

give passive hearing protection its dampening characteristics. Passive protection is preferred over active protection because it is more available, lower cost, and less likely to be faulty due to its lack of electrical components. The structure of the lattice of the actual material along with the physical design of the earplugs combine to give passive hearing protection its dampening characteristics. There are several different kinds of passive hearing protection that are popular on the market currently. In 2014, the Air Force and the Oak Ridge Institute for Science and Education categorized current passive hearing protection into four groups: flanged earplugs, foam earplugs, banded hearing protection and level-dependent earplugs [23]. Visual examples of each type of passive hearing protection currently on the market can be seen below in Fig. 5 through Fig. 8.



Figure 5: Examples of Various Triple Flange Earplugs Currently on the Market [23]



Figure 6: Examples of Various Level-Dependent Earplugs Currently on the Market [23]



Figure 7: Examples of Foam Earplugs Currently on the Market [23]



Figure 8: Examples of Banded Hearing Protection Currently on the Market [23]

Current ear protection effectiveness is measured in Noise Reduction Rating (NRR). This rating classifies a hearing protection device's potential to reduce noise in dB. The higher the NRR the greater the potential for noise reduction. Most passive ear protection has NRR between 22-33; however, it is not as simple as subtracting the NRR rating from the dB exposure level to attain the actual level of dB reaching the ear canal. To determine the actual amount of decibel deduction applied, Eq. 5 can be used to calculate the NRR rating of a hearing protection device. In this equation, the Noise Reduction Rating is the NRR, and that value is subtracted by seven then divided by two. This value is the actual amount of decibel reduction the hearing protection can provide. Equation 4 is for decibel reduction [24],

$$dB \text{ Reduction} = \frac{NRR-7}{2} . \quad (4)$$

Passive hearing protection, such as earplugs, attenuates sound in a linear manner to reduce loud sounds to safer decibel levels; however, they have the same effect on important low intensity sounds such as verbal commands. New technology has pushed passive hearing protection into the nonlinear field of attenuation, attenuating high-intensity sounds relatively more than low-intensity sounds [19]. One example of nonlinearity in passive physical structures is narrow diameter vents which have particle velocity-dependent impedance.

2.3.2 Current Testing of Passive Hearing Protection Devices

The two most common methods to test passive hearing protection devices are called real-ear attenuation at threshold (REAT) and microphone in real-ear testing (MIRE) [25]. REAT is considered the gold standard for testing passive hearing protection systems by the ISO 4869-1 Standard [26]. The REAT is conducted by subjecting an individual to a hearing test with and without hearing protection. However, it is considered a subjective method because the fit of the hearing protection device affects its ability to attenuate noise. Tests in which the experimental officials inserted the hearing protection device for the subject yielded better results than when the test subject inserted the hearing protection themselves [25].

The microphone in real-ear testing (MIRE) is used to measure the hearing protection's field ability with the accuracy and speed of a lab test. In this test, a microphone is placed in the ear to measure the sound levels by the eardrum [26]. Similar to the REAT test, the attenuation levels of the hearing protection device are determined by comparing the results of a hearing test with and without a hearing protection device inserted in the ear. There is a version of the MIRE test, the FMIRE, that ensures a proper fit of the hearing protection device in a field or occupational setting.

2.3.3 Material Properties of Hearing Protection Devices

The materials that make up the physical structures of an earplug are a crucial part of its ability to attenuate sound along with the physical design of the earplugs. Leading earplugs today are made up of damping materials such as plastics, resins, PVC/PU foam, wax, silicone, and vinyl. These materials are polymers which all have varying damping characteristics. Measuring the acoustic attenuation of these materials will be the main focus in our project to be able to create design parameters for passive hearing protection. Acoustic attenuation depends on how a sound wave propagates through a particular medium. Currently, the most frequently used attenuating materials are viscoelastic polymers. As a sound wave propagates through a medium, its intensity decreases with the distance traveled. This phenomenon is referred to as sound attenuation (or acoustic attenuation). The amplitude change of a decaying wave is described by Eq. 5 [27],

$$A = A_0 e^{-\alpha d} , \quad (5)$$

where A is the reduced amplitude at another location, A_0 is the amplitude of the propagating wave at a given location, α is the attenuation coefficient in $\frac{\text{Neper (Np)}}{\text{length}}$, which can be converted to $\frac{\text{dB}}{\text{length}}$ by dividing by 0.115, and d is the distance traveled between the two locations.

Energy absorption and scattering are two key elements of sound attenuation in polymers. Scattering is the result of inhomogeneities in a material such as crystal discontinuities, grain boundaries, inclusions, particles, and voids. However, scattering has little effect in comparison to absorption in polymers. Absorption is the process in which sound energy is converted to heat by elastic motion of particles. When a material is elastically loaded, it stores elastic energy when it is unloaded, some of the mechanical energy is lost and converted to heat. A physical representation can be seen from a stress-strain curve during the loading and unloading of material in Fig. 9 [28].

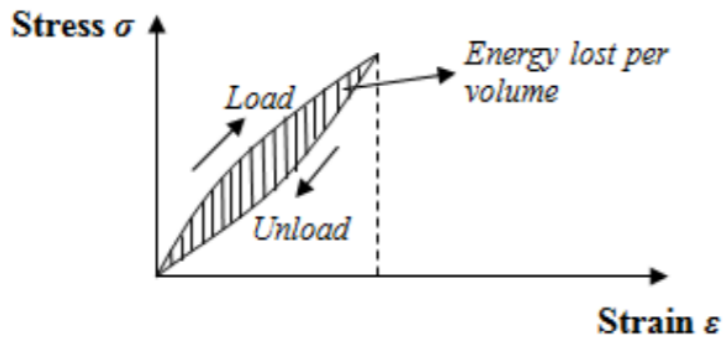


Figure 9: Energy Loss Stress-Strain Curve [28]

The fraction of the energy lost to energy stored is expressed by the damping coefficient η , also known as $\tan(\delta)$, the loss factor, or mechanical loss coefficient, which signifies the degree to which a material dissipates or absorbs vibrational energy. $\tan(\delta)$ can also be thought of as the ratio of the loss modulus E'' to storage modulus E' during the loading and unloading of a material shown in Fig. 10.

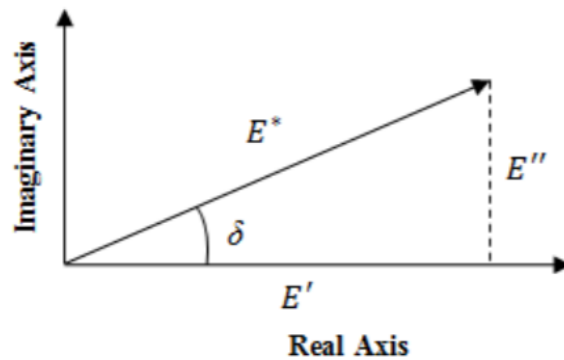


Figure 10: Damping Coefficient [28]

Below are two tables [28]. The first, Table 2, is a table of different thermoplastics and their relative $\tan(\delta)$, or damping coefficients. The second, Table 3, is a table of acoustic properties of common polymers.

Table 2: Damping Coefficients of Thermoplastics [28]

Material	$\tan \delta$
Thermoplastics	
EEA (Ethylene Ethyl Acrylate)	0.774
PVC, soft, A60	0.68 - 1.6
EMA (Ethylene Methyl Acrylate)	0.585
EVA (Ethylene Vinyl Acetate)	0.5
EBA (Ethylene Butyl Acrylate)	0.48
FEP (Fluorinated Ethylene Propylene)	0.11
Ionomer	0.1
PTFE (Teflon [®])	0.07 - 0.1
UHMWP (Ultra High Molecular Weight Polyethylene)	0.041 - 0.045
PP (Polypropylene)	0.03 - 0.04
ASA (Acrylonitrile Styrene Acrylate)	0.0184
PC (Polycarbonate)	0.016 - 0.017
PVC (Polyvinyl Chloride), rigid	0.016 - 0.017
ABS (Acrylonitrile Butadiene Styrene)	0.0145 - 0.0183
PMMA (Acrylic)	0.012 - 0.018
PA (Nylon)	0.01 - 0.03
Thermosets	
Polyester, flexible	0.13 - 0.137
Epoxy, standard	0.016 - 0.017
Thermoplastic Elastomers (TPE)	
PVC elastomer	0.2 - 0.5
Thermoset Elastomers (Rubber)	
Fluoro elastomer	1.34
Butadiene rubber	0.065 - 0.13
Neoprene rubber	0.06 - 0.17
Polyurethane rubber	0.05 - 0.1

Table 3: Acoustic Properties of Polymers [28]

	Longitudinal Velocity m/s	Acoustic Impedance MRayl	Attenuation dB/cm @ 5 MHz
Polyurethane rubber	2090	2.36	27.6 - 100
Polycarbonate (Lexan)	2300	2.75	23.2
Epoxy	2360	2.86	15 - 20 [36]
Nylon 6-6	2600	2.9	12.9
Acrylic, clear	2750	2.32	11.3
Type I PVC	2270	3.27	11.2
Polyester	2290	2.86	10 - 20 [37]
UHMWP	2364	2.33	8 [38]
Polypropylene	2740	2.4	5.1
Teflon [®]	1390	3	3.9
Polystyrene	2400	2.52	1.8

2.4 Overview of Past MQP

A previous MQP team completed a project that designed and created an ultra-high-speed shock tube with the intent to research Tympanic Membrane fractures. Utilizing the high-speed shock tube and high-speed imaging techniques the team was able to characterize density differentiation in shock waves. The shock tube has the ability to output blasts of different magnitudes based on what is desired by changing the diaphragm, which separates the driving and driven sections. The creation of this shock tube will allow for the study of passive hearing protection with non-linear sound waves to properly account for the variety of stimuli the ear can be exposed to [29]. The ultra-high-speed shock tube characterization is shown in Fig. 11.

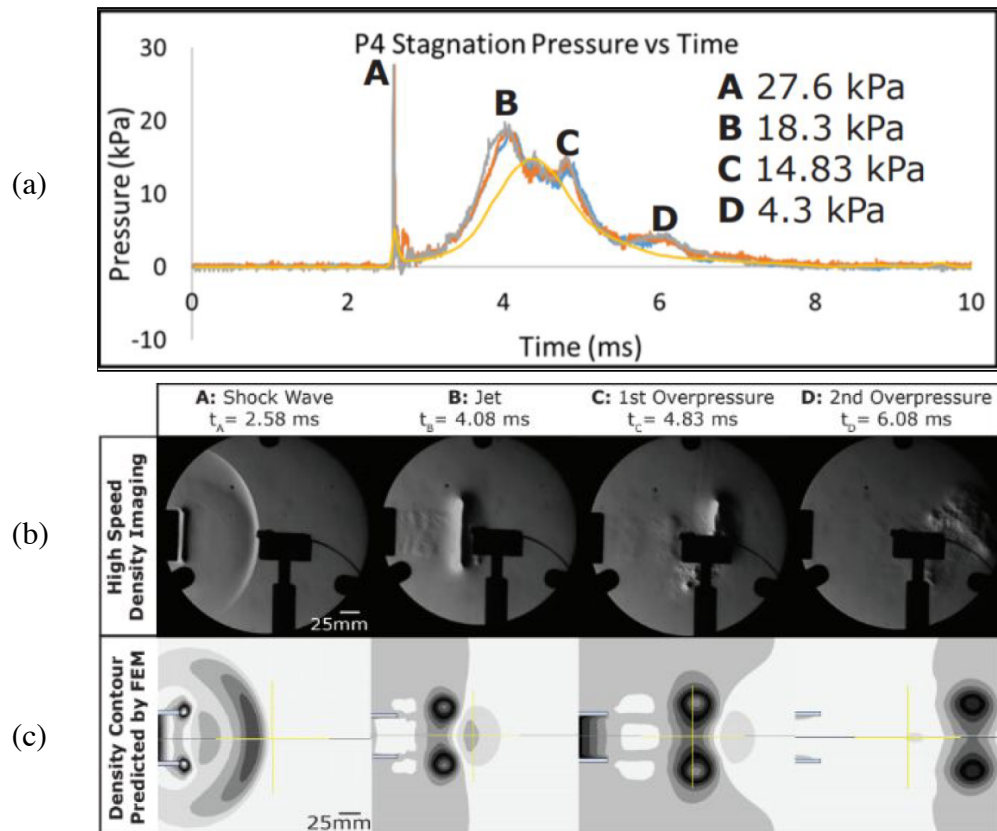


Figure 11: Experimental and Computational Results Obtained with a Shock Tube [29]. (a) High-Speed Measurements of Acoustical Pressure; (b) High Speed Schlieren Imaging; (c) Computational Analysis

Through experimental and computational work, the team characterized the output of their shock tube. Schlieren imaging was used to correlate the pressure data to the experimental shock wave in real time. The previous team developed a LabVIEW program that would record pressure data at four points that can be seen in Fig. 11. Through the imaging and the data collected from the LabVIEW program, the team was able to observe, both visually and quantitatively, the stages of a shock wave. The first wave seen is the shock wave, followed by the jet, and then the sound pressure wave that collects behind the diaphragm before rupturing it. The shock tube produced repeatable waves at 150 dB SPL or higher and was able to rupture a human tympanic membrane.

Building on the work of a previous MQP team, our team will advance the research into passive hearing protection and the damping characteristics of different material properties. In the next chapters, we will outline our methodology, results, and conclusions of our experiment.

3. Methodology

In this project, we developed a methodology to investigate the limitations of current passive hearing protection analytically, experimentally, and computationally to examine the relationships between microstructure, macrostructure, and performance. Based on a review of the literature, our team developed and applied a testing apparatus and methods to isolate specific earplugs samples in order to assess their performance by measuring their corresponding Frequency Response Functions (FRFs) under sustained noise. The FRFs were analyzed and used to understand differences in attenuation between samples and to identify limitations in their acousto-mechanical design parameters. Concurrently, computational models were developed to parametrically investigate how microstructure, material properties, and earplug geometries attenuate different sound pressure levels and frequencies.

3.1 The ANSI Standard

The American National Standard for testing hearing protection is laid out in a document known as the ANSI S12.6. The current standard for testing passive hearing protection devices uses human subjects and breaks them into two testing groups: trained subject fit and inexperienced subject fit. During our experiment, we didn't test on human subjects. Instead, we manufactured a pinna fixture that adheres to the ANSI S12.6 standard to hold the passive hearing protection sample. The drawing for the ANSI S12.6 pinna fixture can be seen below [30].

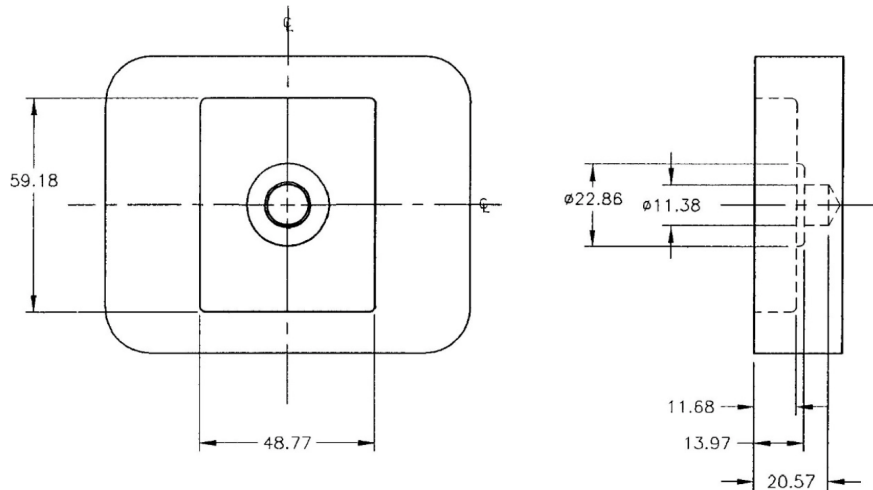


Figure 12: Drawing for ANSI S12.6 Pinna Fixture [30]. This schematic was used to create a CAD model in SolidWorks which was then used to manufacture the pinna fixture in the WPI Manufacturing Labs using a Mini Mill Machine

The fixture was manufactured out of aluminum 6016 and was modified to incorporate a mock ear canal. The dimensions of this modification were modeled after the average length and diameter of a human ear canal.

It was evident that the earplugs needed to be tested in a variety of ways, including the shock tube previously mentioned. For this reason, the experimental setup needed to be adaptable to account for different distances, heights, etc. for each test. We decided that in each test the sound stimulus would be directly facing the testing fixture, so the experimental setup did not need to be adaptable in this parameter. To optimize the reliability of the test, it was important that the testing setup moves as a unit.

3.2 Experimental Setup

The next step was to develop the experimental instrumentation to properly test the earplug samples in the ANSI S12.6 adapter. Based on previous research, an acoustic testing system was developed with the ability to measure the sound pressure attenuation of the earplug samples. An artificial pinna fixture was modified and manufactured to hold an earplug in place while it is being subjected to a frequency sweep. One pressure sensor was located in the front of the earplug and one was located behind the earplug in the artificial pinna. This setup was enclosed in a sound absorbing box in order to minimize interference. The responses from the two microphones were

recorded and the corresponding Frequency Response Functions (FRFs) were calculated. This procedure was performed on multiple earplugs with different microstructure and geometry. The physical apparatus was designed concurrently with the software and data analysis techniques to measure the Frequency Response Function. An anechoic chamber was designed to enclose the measurement instrumentation for the acoustic experiment. The data from the experiment was acquired and analyzed using LabVIEW software.

3.2.1 Selection of Passive Hearing Protection

For this experiment, our team selected five different types of passive hearing protection with the goal of characterizing each sample's performance with respect to their micro and macrostructure. Three foam earplugs were chosen in order to study microstructure and two earplugs that rely on macrostructure were chosen to study the effect of geometry on attenuation. The industry standard for general characterization of these earplugs is their respective Noise Reduction Rating (NRR) rating. The first two samples are standard polyurethane foam earplugs with similar shapes designed for very similar attenuation capabilities, the only difference is that Sample 1 has a slightly higher NRR. The third sample is made from a porous foam similar to the first two samples, however this sample was designed for less intense sustained noise that would be common in the industry. Sample 4 has a tri-flange shape that differs greatly from the shapes of other samples. The fifth and last sample is a silicon material and is a moldable earplug to various shapes and sizes. These five samples were chosen to compare materials with different porosities and shape to characterize the performance. The five samples can be seen in Fig. 13.



Figure 13: Passive Hearing Protection Samples. Samples 1 through 3 are porous earplugs that rely on porosity to attenuate sound. Sample 4 and 5 are earplug samples that rely on macrostructure to attenuate sound

3.2.2 Testing Apparatus Development

In order to get repeatable and reliable data, multiple components were manufactured and assembled. As mentioned previously, we manufactured a pinna fixture per the ANSI S12.6 standard. A SolidWorks model of the pinna fixture is shown in Fig. 14. The model was adapted to allow for the pinna fixture to be fixed securely to the rest of the setup and to allow for a pressure sensor to be secured to the end of the artificial pinna. Threaded holes were added to the bottom of the model in order to bolt the fixture securely to the setup.

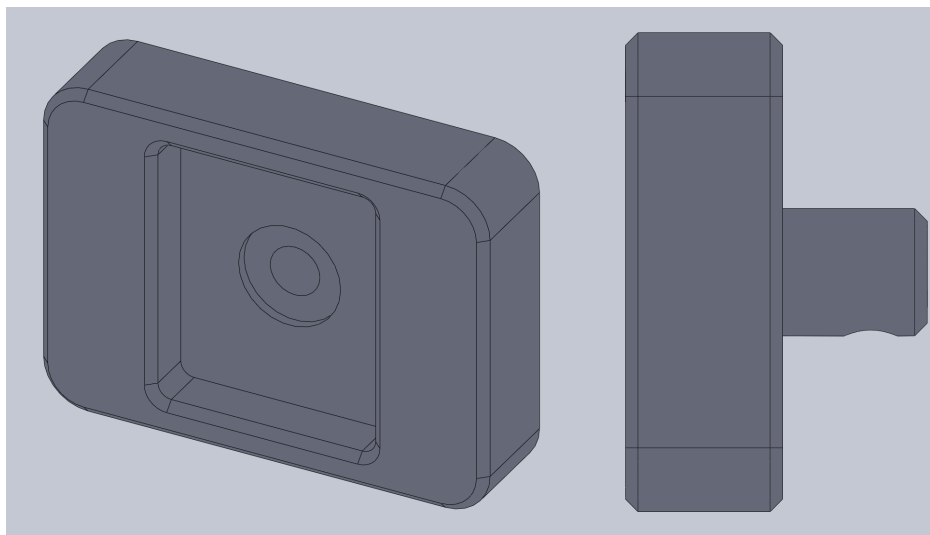


Figure 14: SolidWorks Model of ANSI S12.6 Pinna Fixture: Isometric View, Side View. This is the SolidWorks CAD model that was used to manufacture the pinna fixture in the WPI Manufacturing Labs

A threaded hole was bored through the back end of the artificial pinna so the pressure sensor can be secured, shown in Fig. 15. The goal of positioning the pressure sensor in this location was to measure the sound pressure level that the temporal membrane is subjected to. The sensors selected were the 102B06 Model from PCB Piezotronics. These were selected because of their sensitivity of 1.45 mV/kPa and their ability to handle high pressures (68,950 kPa).

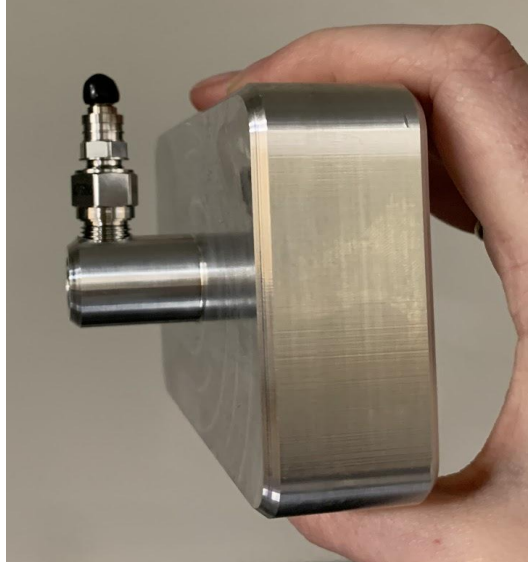


Figure 15: Pinna Fixture Precision Manufactured and Customized to Introduce Additional Sensor

The adjustable platform is a plate that can be adjusted to a desired height and location while also remaining fixed to the experimental table, shown in Fig. 16. The adjustable platform was put on tracks in order to allow for control of the location of the pinna fixture. The tracks allowed for the system to be moved anywhere on the two-foot-long track accomplishing the adaptable aspect required for the setup. The adjustable platform on the tracks allows for a height range of three to nine inches above the table. The adjustable height and sliding rails are important when utilizing the shock tube nonlinear testing because the intensity of shockwaves is greatly affected by the distance from the source. For example, a blast from directly in front of the shock tube exit can reach up to 196 dB SPL but drops to 170 dB SPL 12 inches from the exit. This platform, which can be seen in Fig. 16, allows for researchers to choose which sound level they want for an experiment.

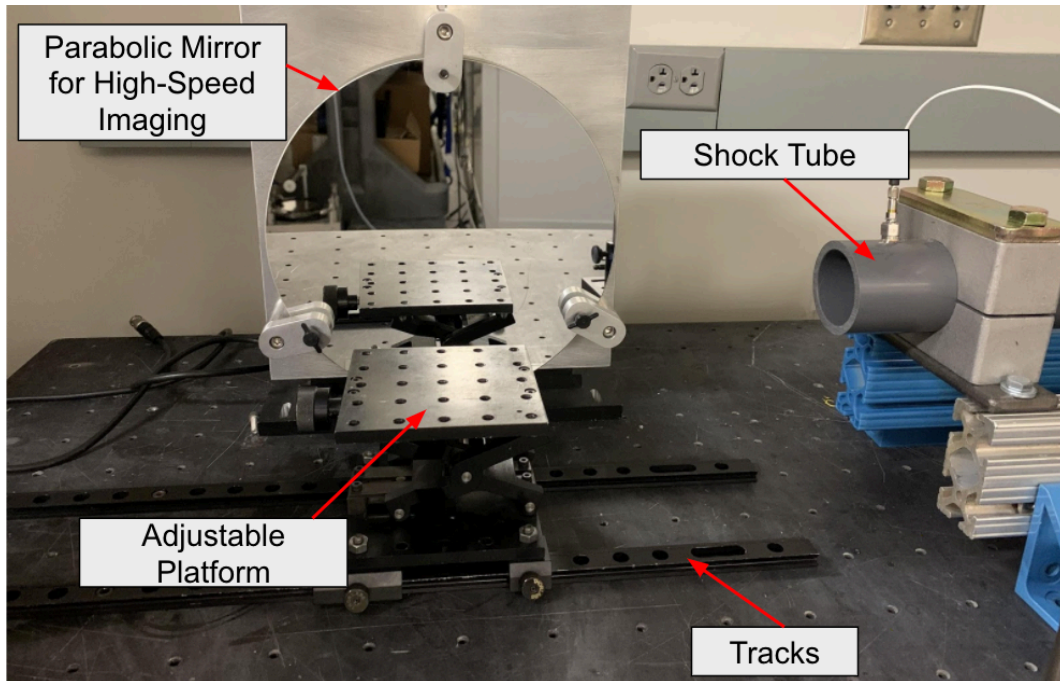


Figure 16: Platform and Tracks Used in the Experimental Setup that Allowed for Adjustable Distance and Height. Shock Tube and Parabolic Mirror for High Speed Imaging also Pictured

A 4 by 6-inch plate was designed and manufactured to connect the pinna fixture to the adjustable platform. This mounting plate ensures that the adapter will not move during testing or cause unreliable data. A $\frac{3}{8}$ -24 threaded hole was tapped into the plate for the flexibility to mount a pressure sensor. The pressure sensor can be screwed into the plate, ensuring equal distance from the pinna fixture to where the pressure measurement is taken for every test run. This plate, which can be seen in Fig. 18, ensured repeatable testing and allowed the entire test system to move as one unit. Similarly, the pinna test fixture was detailed with a threaded hole in the simulated ear canal that matched the thread of the pressure sensors. Again, this ensured repeatability of the distance of where the pressure measurement was taken and allowed the entire test setup to move as a unit. A completed experimental setup can be seen below in Fig. 17.

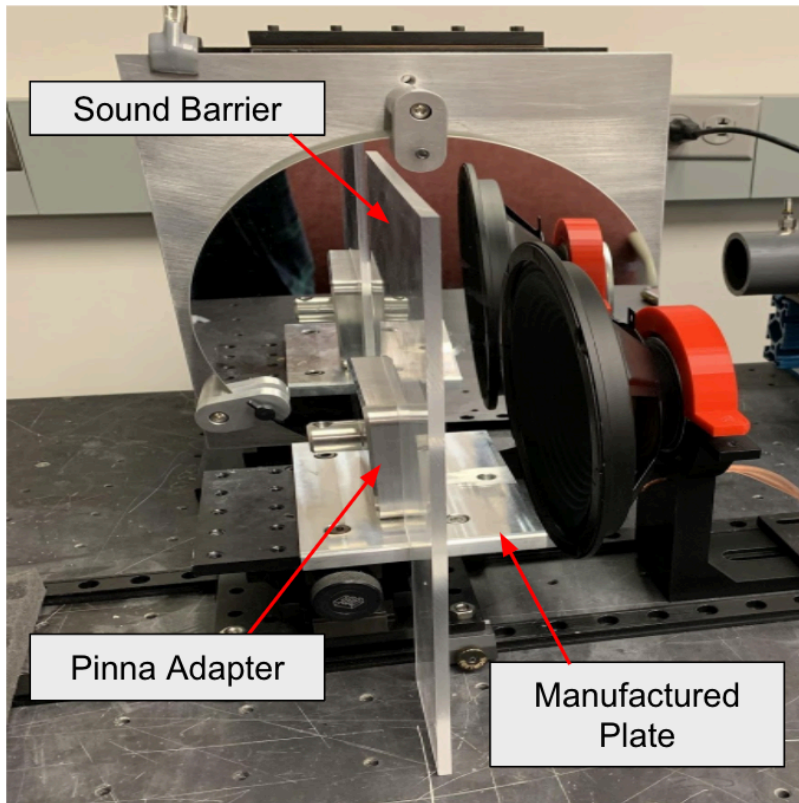


Figure 17: Pinna Fixture on Adjustable Platform with Sound Blocking Barrier, Custom Manufactured Mounting Plate, and Speaker

As stated previously, the pressure sensors used in this experiment are extremely sensitive, so it was important to isolate the experiment as much as possible. First, a sound barrier was constructed with the purpose of blocking the sound waves from traveling around the adapter and interfering with the microphone placed on the rear of the adapter. The barrier was made from a polycarbonate sheet, $\frac{1}{2}$ in thick so that it would not bend or break when different pressure sources were utilized on the system. The barrier was then covered in sound-absorbing foam to further dampen the incoming frequencies. A SolidWorks model used to manufacture the sound barrier can be seen in Fig. 18.

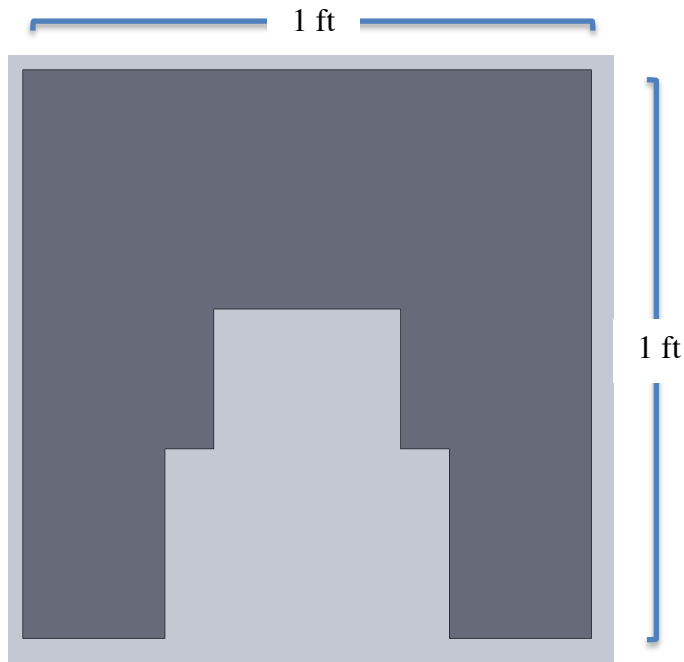


Figure 18: Sound Barrier Manufactured for Experimental Setup, 1 ft by 1 ft. The Barrier Fits Within our Enclosure with Cutouts for the Adjustable Platform and Pinna Fixture

In addition to a sound barrier placed around the fixture, an isolating chamber was designed to enclose the entire experimental setup. The purpose of this was to eliminate the external disturbance and add consistency and repeatability to the experiments. Knowing that the Schlieren system would be used in future experiments and need to be accessible, the chamber was designed with removable sides to allow the camera and laser to be able to interact with the mirror on the other side of the experimental setup. The sides were attached using chest latches, as opposed to hinges, due to the proximity of the Schlieren and the size of the chamber. The chamber, similar to the sound barrier, is made out of a polycarbonate sheet. The entirety of the inner surface area of the chamber was lined with sound-absorbing foam to further reduce possible disturbances in data collection. An image of the completed experimental setup can be seen in Fig. 19.

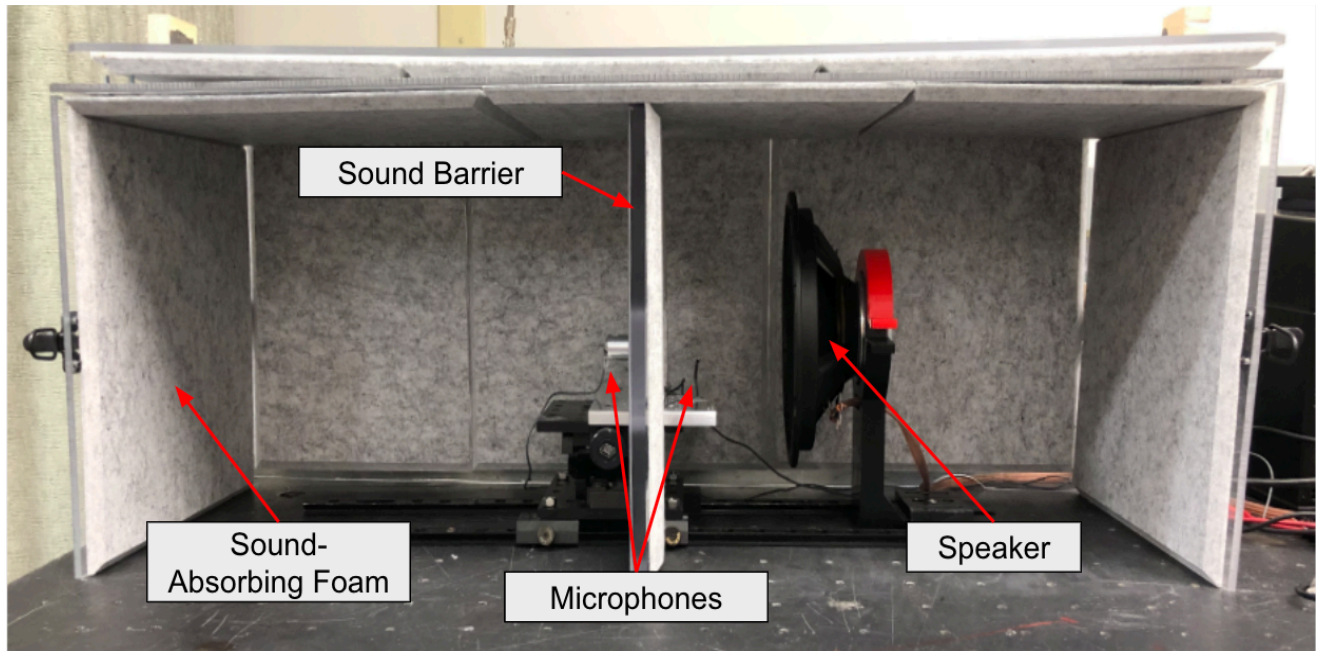


Figure 19: Complete Experimental Setup With Anechoic Chamber, Sound Absorbing Foam, Microphones, Sound Blocking Barrier and Speaker

3.2.3 Frequency Sweep Experiment

In order to properly measure the responses of the passive hearing protection devices, we subjected each sample to a frequency sweep stimulus and recorded the sound pressure at the input and output of the earplug system. The recorded pressure was changed from the time domain to the frequency domain with a Fourier Transform shown in Eq. 6. In this equation, $f(t)$ is the input function, i is the imaginary number, ω is the angular frequency, and t is time. The Fourier Transform equation [31] is,

$$F(\omega) = \int_{-\infty}^{\infty} f(t) e^{-i\omega t} dt . \quad (6)$$

In this experiment the earplug acts as the system being analyzed and the measurements will be taken at the input and output of the system. The input of the system was a sweep of frequencies from 1-10 kHz outputted by a standard dual-channel function generator to a Celestion 8” diaphragm speaker. This frequency range was chosen because it includes lower more common frequencies (1,000-4,000 Hz) and higher damaging frequencies (4,000-10,000 Hz). The data was acquired by two microphones, one at the input and one at the output of the system. Each microphone recorded $\frac{\text{Voltage}}{\text{Time}}$ and was analyzed in LabVIEW. The linear $\frac{\text{Voltage}}{\text{Time}}$ data was transformed into the frequency domain using a Fourier Transform in LabVIEW to properly assess the sound pressure levels at each frequency over the spectrum. The partial LabVIEW wire

diagram of the implemented code is shown in Fig. 20. For the entire code, see Appendix C. According to the diagram, sensors that are placed at the input and output of the system are wired into an FRF signal processing unit in LabVIEW. The FRF function takes two inputs and outputs the FRF, coherence and phase functions to graphs that can be easily read in the front panel.

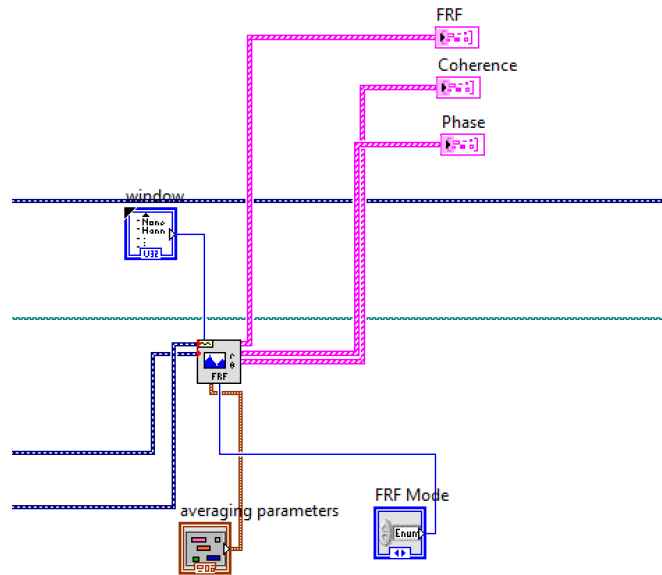


Figure 20: LabVIEW Block Diagram FRF Function

The LabVIEW program calculated each individual Fourier transform and plotted the graphs at the top of the front panel. The two graphs on the left show raw microphone data of the front and back. The graphs on the right show the corresponding Fourier transform data. These are depicted in Fig. 21.

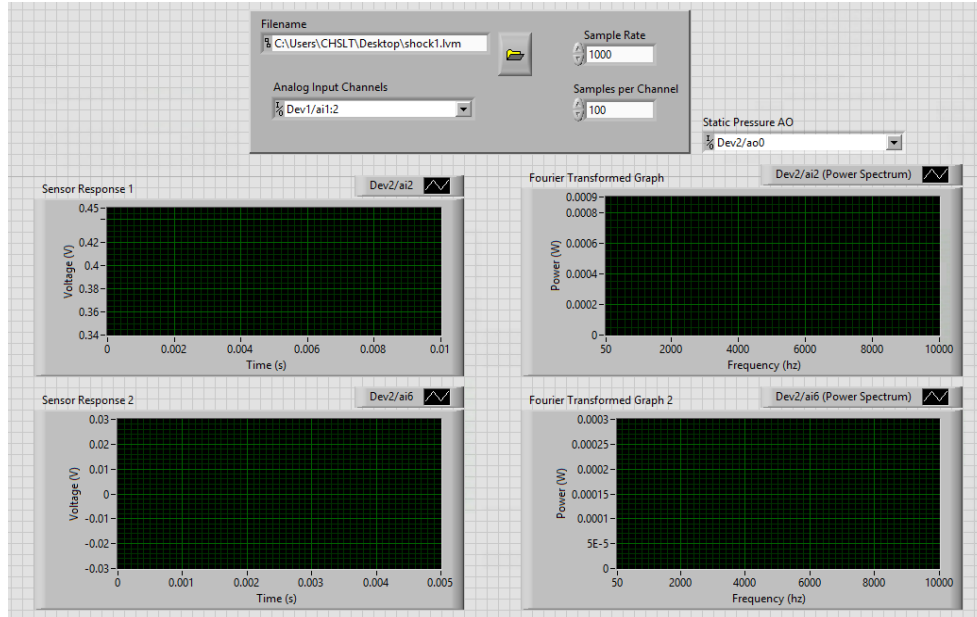


Figure 21: LabVIEW for Sweep Experiment Front Panel. Top Inputs are for Sampling Rate, Samples per Channel, Input Channels and Output File Name. Graphs Below Display Uncalibrated Microphone Response and Fourier Transform Data

After each microphone data was recorded and transformed into the frequency domain, the ratio of the two responses ($\frac{Output}{Input}$) was taken to obtain the Frequency Response Function (FRF) of the system. The FRF is calculated by dividing $F(f)'$ by $F(f)$, $\frac{F(f)'}{F(f)}$, in our system. The FRF of each sample allowed the team to identify which frequencies are damped by the earplug and how much each sample attenuates comparatively.

3.2.4 Anechoic Chamber Development and Verification

The computational analysis of the experimental setup was created and optimized to ensure the validity of the data through the use of a parametric study. COMSOL was chosen to complete this analysis because of its capability to analyze acoustics in the frequency domain. This capability allowed for the computational data to be compared to the experimental data. The first part of the computational model is the ANSI S12.6 Pinna Fixture, seen in Fig. 22. The adapter was modeled to represent the experimental adapter; however, the geometry was simplified for the preliminary calculations. The adapter was made to be a solid domain and the material was Aluminum 3003-H18. The bottom surface of the pinna fixture was fixed in the model, meaning it was constrained in the x, y, and z-directions as well as rotationally about the x, y, and z-axis. This replicates the

real constraints of the experiment as the adapter is rigidly connected only on its bottom surface to the mounting plate.

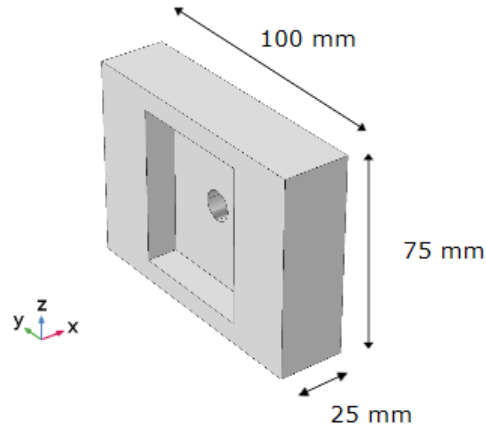


Figure 22: CAD Model of Pinna Fixture Used in COMSOL to Complete the Computational Analysis

The second part of the computational model is the passive hearing protection, seen in Fig. 23. The hearing protection, or earplug, in the experimental setup is made of polyurethane foam and is reflected in the computational model. The earplug was modeled as a poroacoustic domain. This domain uses Biot's theory to calculate wave propagation through porous materials [33]. The purpose of this simulation was to understand the effect of enclosure size on pressure variation, so the earplug was modeled simply as a standard polyurethane foam. This cylindrical geometry sits inside the pinna fixture, analogous to the experimental setup, and was fully constrained for simplicity.

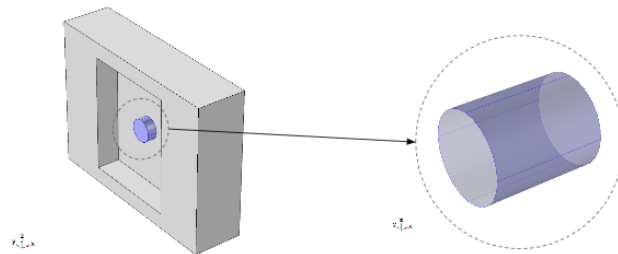


Figure 23: COMSOL Model of the Pinna Fixture With Inserted Earplug

The sound barrier was the next part of the computational model, seen in Fig. 24. The barrier was modeled as a solid domain and was made of $\frac{1}{2}$ inch polycarbonate sheet. The experimental setup has a layer of sound-absorbing foam. For this reason, the barrier was made to have a sound soft boundary. This boundary is a type two boundary condition that allows the pressure gradient to go to zero at these boundaries [32]. The barrier was constrained in the x, y, and z-direction as well as rotationally about the x, y, and z-axis similar to the adapter.

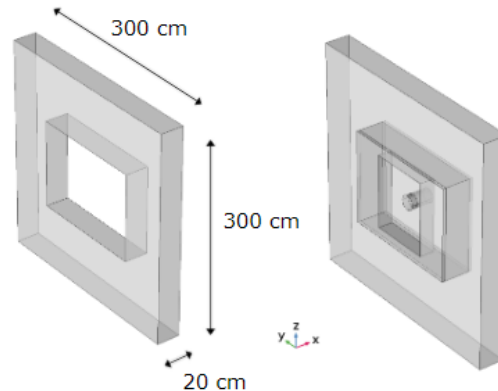


Figure 24: CAD Model of the Sound Barrier Used in COMSOL to Complete the Computational Analysis

The last part of the computational domain is the volume of air around the adapter, hearing protection, and barrier, seen in Fig. 25. In this boundary, a sound pressure point source produced the sound pressure. This point source was located 10 cm from the front of the adapter. The boundary of this domain was made to be sound soft, like the barrier, in order to represent the sound-absorbing foam on the inside of the chamber of the experimental setup. The computational and mesh convergence was found by testing various sizes of the domain and various sizes of mesh.

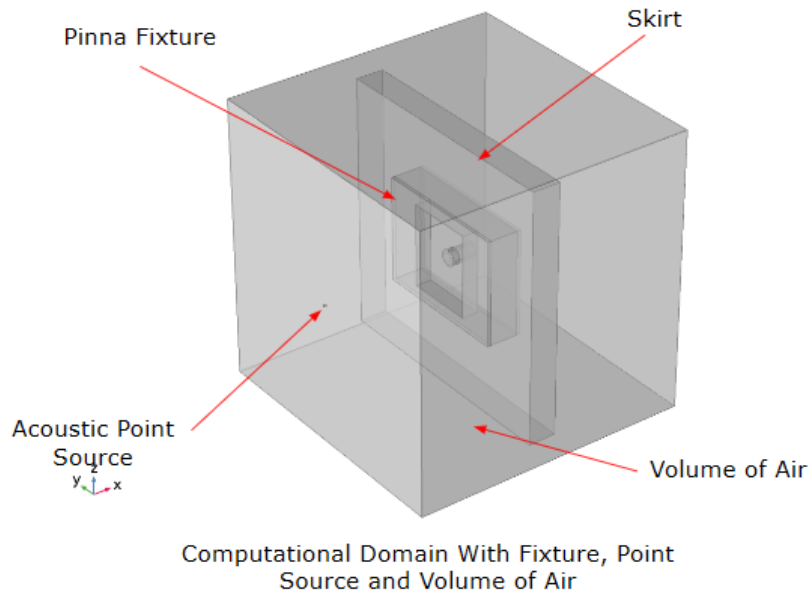


Figure 25: Completed Model of Enclosure, Sound Blocking Barrier, Pinna Fixture and Earplug

This setup was tested with different geometries for the box surface. Shown in Fig. 26 are the four different sizes that were studied.

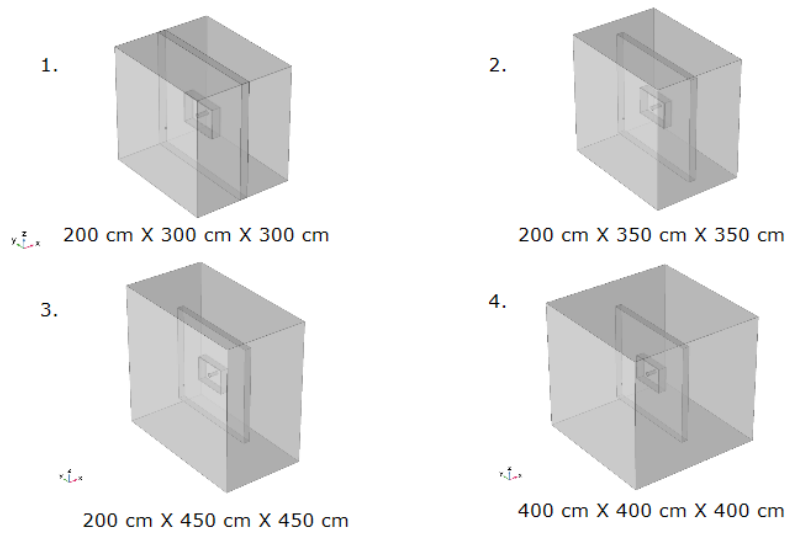


Figure 26: Four Different Enclosure Geometries Tested for Accuracy of Computational Model

The setup was subjected to a sound pressure of 147 dB SPL at 2000 Hz from the point source. The sound pressure level was recorded 2 cm from the front and the back of the fixture, and a pressure drop of 20 dB SPL was observed. Fig. 27 shows the pressure distribution in the box at a plane located in the middle of the box.

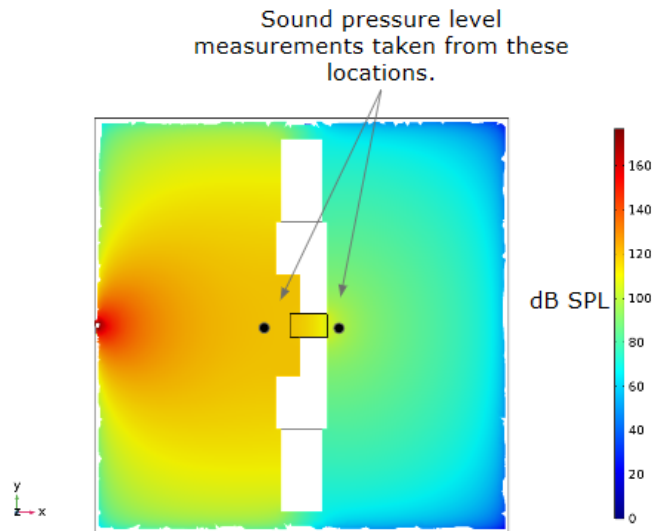


Figure 27: Pressure Distribution within Simulated Enclosure with Point Source and Sound Blocking Barrier

This simulation was done for each geometry and the results were plotted against each other shown in Fig. 28. The purpose of this study was to understand how enclosure size would have an effect on the pressure readings at the front and back sensors. The enclosure was tested at four sizes to understand the minimum size that would create a convergence. As seen in Fig. 29, as the volume increases from around 23,000 cm³ to 30,000 cm³, the pressure increases nearly 20 dB SPL as well. From 30,000 cm³ to 65,000 cm³, the pressure remains consistent, showing 30,000 cm³ as an appropriate enclosure size.

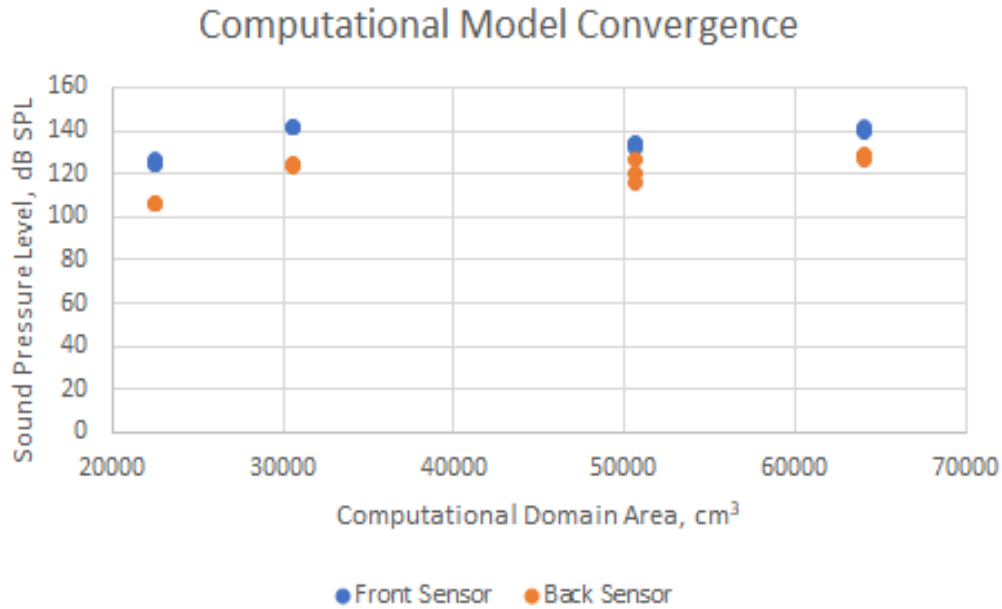


Figure 28: Convergence Plot Showing Effect of Enclosure Size on Earplug Front and Back Pressure Measurements

These results showed that the size and geometry of the box converges at a volume of 30,000 cm³. The mesh size was shown to converge at a maximum element size of 10 mm. Based on the area at which the model converges, the experimental setup was designed.

3.3 Understanding the Microstructure and Macrostructure of Hearing Protection

The earplugs that were tested were divided into two main groups, porous and non-porous. For the porous earplugs, we used a Keyence VHX 7000 microscope to capture the microstructure of each sample. This microscope has the ability to build a composite picture of multiple layers of a 3D image into a clear, 2D image. We used this feature on each of our earplug samples. Not only was the microscope able to capture the topology of each earplug, but it also constructed a 3D version of the topology. The earplug samples were cut to find the horizontal and vertical profiles of the porous microstructure. An example of the image collected for each sample is shown in Fig. 29.

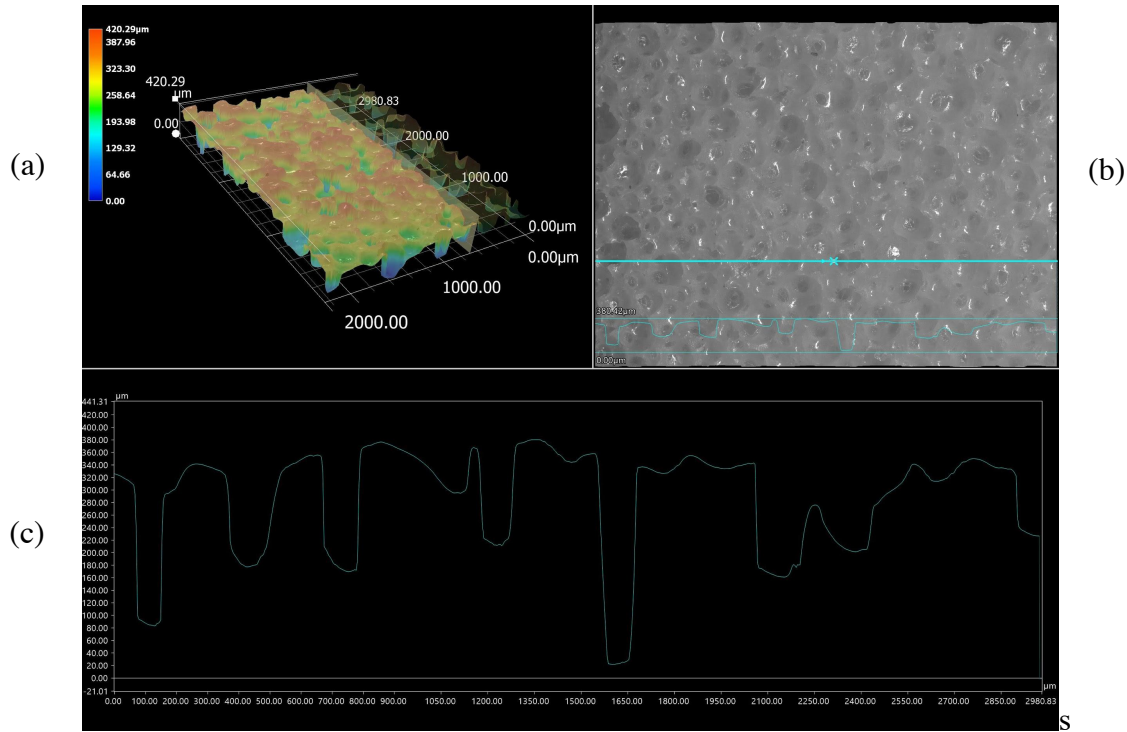


Figure 29: Sample 1 Observed Under 100x Magnification. (a) 3D Elevation; (b) Greyscale Image of Porous Structure; (c) Representative Cross-Section Showing Elevations

In addition to the visualization of different profiles, the microscope software exported a data file that showed the depth, in microns, of each of the pores in that profile. This data was used to find the average pore size and the number of pores in each plug. The average pore size and the number of pores in each plug were then used to calculate an approximate volume of air within each plug. These steps can be seen in Appendix E. The value of air in each plug was then used to compare the performance of the earplugs and act as reference values for the parametric studies conducted in COMSOL.

To understand the macrostructure, the non-porous earplugs were examined, since their main mode of attenuation was geometry. To see the macrostructure of the hearing protection, the sample was looked at using the naked eye, then bisected to see the cross section. The shapes of the non-porous earplugs were split into two main groups and implemented in the computational model.

3.4 Computational Model

To complement our experimental study, we created a model in COMSOL simulating a pressure input interacting with an earplug. For the porous earplugs, this model was used to understand the

effect of varying material properties on the sound-absorbing qualities. A separate model was created for triple-flange earplugs to study the effect of each flange on overall attenuation.

3.4.1 Purpose

The purpose of this model was to gain an understanding of how various material properties affect attenuation. The fundamentals of acoustic absorption state that porosity and pore structure are critical to energy absorption. This model was used to confirm the magnitude of this effect. As opposed to the full chamber model, this is a focused analysis of solely the earplug. To maintain consistency between testing, the input pressure was similar to the testing speaker stimulus, keeping the earplug attenuation in the linear range.

Additionally, for the tri-flange earplugs we hoped to gain a visual understanding of how the macrostructure affected attenuation. We did not plan to vary tri-flange material properties but rather look at the pressure profile to determine how the pressure varies through the flanges.

3.4.2 Governing Equations

The computational model was built in the acoustics module of COMSOL and analyzed in the frequency domain. Before building the physical mode, we worked to understand the governing equations used to solve the material response. To simulate a porous material, we used a multiphysics coupling of the poroelastic waves analysis and pressure acoustics analysis. The poroelastic waves method models a porous medium as a single, homogenized material. This is done through the Biot-Allard Theory, shown in Eqs 7 and 8 [33], which uses material properties of both the solid and fluid matrix material,

$$-\left(\rho_{av} - \frac{\rho_f^2}{\rho_c}\right)\omega^2\mathbf{u} = \nabla S = Fv e^{i\phi} + \frac{\rho_f}{\rho_c}\nabla p, \quad (7)$$

$$F(\omega) = \left(1 + \frac{4i\omega\tau_\infty^2\mu_f\rho_f}{R_f^2L_v^2\varepsilon_p^2}\right). \quad (8)$$

In these equations u is the displacement of the porous material, ω is the fluid displacement with respect to the porous matrix, ρ_f is the fluid density, μ_f is the fluid's viscosity, τ is tortuosity, ε_p is the porosity, L_v is the viscous characteristic length, ρ_f is the fluid pore pressure, ρ_c is the porous material density, and ρ_{av} is the average density ($\rho_c + \varepsilon_p\rho_f$) [33]. From these equations, key variables of interest were determined for the parametric study, explained further in Section 3.3.4.

3.4.3 Porous Model Development

After understanding the governing equations, we moved to define the physical model. We determined for simplicity and focused analysis that this model would contain simply an earplug with a 1 cm occluded length of air to simulate the air trapped between the earplug and the eardrum. The biological representation of this model can be seen in Fig. 30.

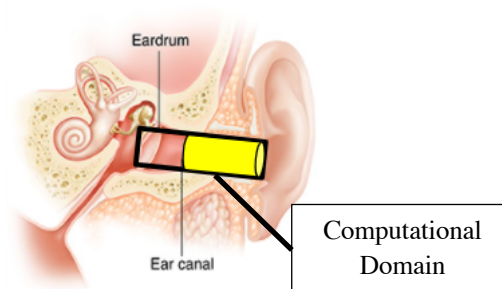


Figure 30: Computational Model in the Context of the Ear

The earplug geometry used for the model is a cylindrical 3M earplug which can be seen in Fig. 31. Polyurethane foam was used as the matrix material and standard values for this material were input for the initial simulation.

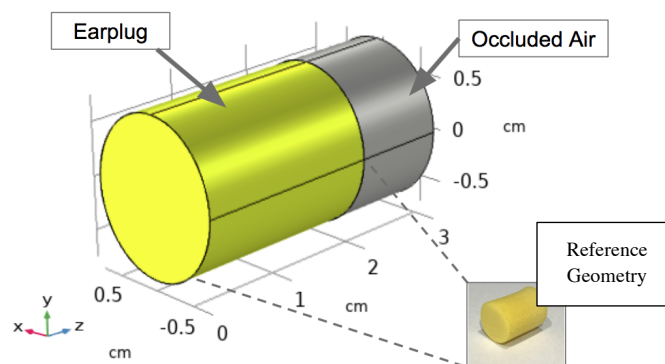


Figure 31: Computational Model of Porous Earplug. Earplug, Shown in Yellow, Based off Reference Geometry. Occluded Air Simulating Air Between Earplug and Eardrum

As shown in Fig. 31, the earplug and occluded air domain are modeled in two different domains. The earplug is modeled with the complex poroelastic wave analysis described in Section 3.3.2, with the air being modeled in the pressure acoustics domain. The boundary between these two domains is treated as an acoustics-porous boundary where the input and output pressure are equal. The various conditions applied to this model can be seen in Fig. 32.

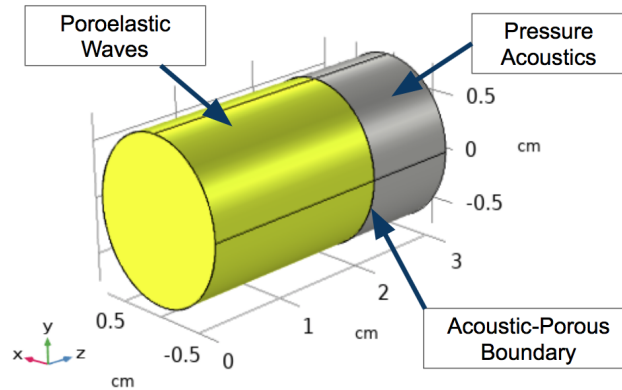


Figure 32: Porous Earplug Multiphysics Domains. Poroelastic Waves Domain Used for Earplug to Model Porous Material. Pressure Acoustics Domain Used for Occluded Air. Acoustics-Porous Boundary Multiphysics Condition Applied at the Boundary

For simplification of the model, the earplug is considered fixed on all sides with all six degrees of freedom constrained. The input and output are modeled as ports that are used to excite and absorb acoustics. In the portion of occluded air, the boundaries are sound soft, meaning the pressure is absorbed as it contacts those surfaces. The input port provides the stimulus, 1 Pa, as a uniform pressure field. The output port is used to measure the reduced pressure. These boundary conditions can be seen in Fig. 33 with detailed images in the Appendix G.

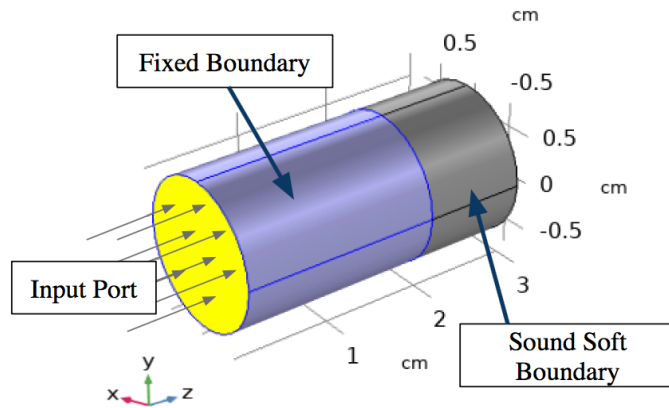
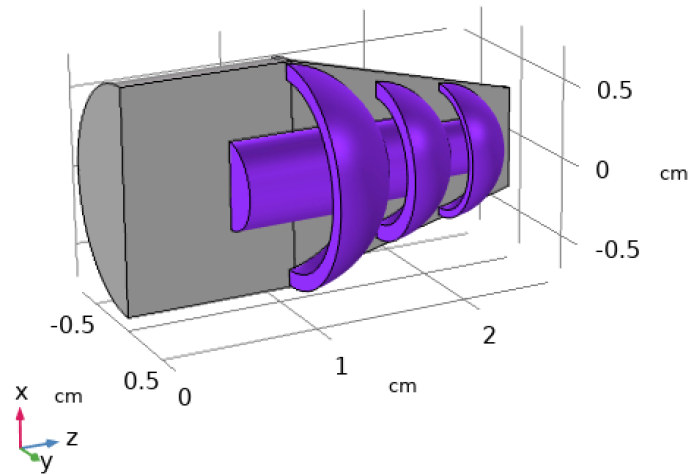


Figure 33: Porous Earplug Boundary Conditions. Earplug Fully Constrained with no Translations or Rotations on the External Surfaces (shown in blue). Input Pressure Applied to Earplug Front. Sound Soft Boundary Conditions Applied to Ear Canal Wall

To analyze the effects of various material properties, we decided to run frequency sweeps from 1 - 10 kHz, which is consistent with our experimental method. From the governing equations, we identified six properties of interest: density ρ_c , fluid density ρ_f , porosity ε_p , viscous length μ_f , shear modulus G , and Poisson's Ratio ν . To analyze the effects of each property, a parametric study was run for each with $\pm 20\%$ of the actual material property. This parametric testing was used to determine which properties were most important, and in which way the properties would affect overall performance.

3.4.4 Triple Flange Model Development

In addition to the porous plug model, we analyzed the triple flange geometry. This model was completed entirely in the pressure acoustics domain. Due to the complex geometry and interaction with the ear canal, some geometric simplifications were applied. When the actual plug is placed in an ear canal, all flanges contact the canal walls. To simulate this, we modeled the ear canal as a partial cone so that air could not freely pass around the plug. This can be seen in Fig. 34.



*Figure 34: Triple Flange Computational Setup.
Imported Triple Flange Geometry Shown in Purple.
Ear Canal Geometry Shown in Grey. Ear Canal Geometry Tapered to Airtight
Boundary with Earplug*

From the geometric model shown in Fig. 34, we created a two-dimensional axisymmetric model as seen in Fig. 35. Since the geometry was completely symmetric, this simplification was appropriate to reduce computational time. At the input of the earplug, which is the large-diameter side, a uniform pressure field of 1 Pa is applied. The walls of the ear canal are modeled as sound hard boundaries meaning that the sound energy is not absorbed at those barriers. A sound soft boundary is placed at the end of the canal which absorbs the remaining sound pressure that is let through the plug.

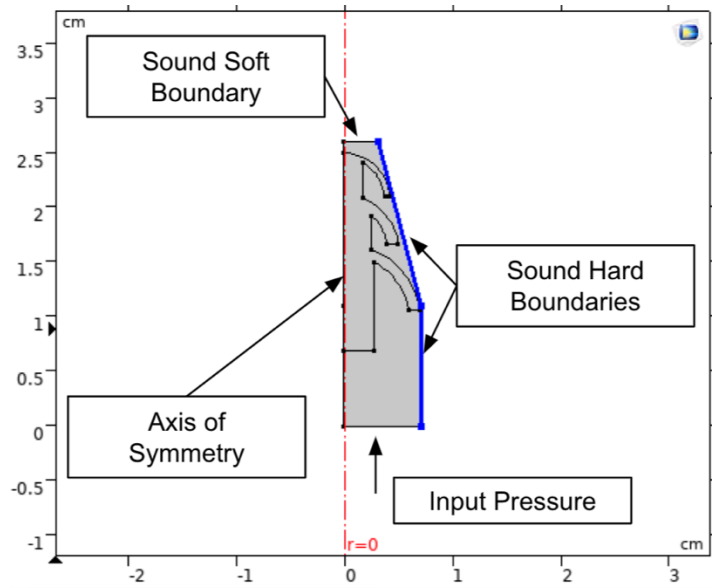


Figure 35: Triple Flange Boundary Conditions. Uniform Pressure Front of 1 Pa at Input. Axis of Symmetry around $r=0$. Sound Hard Boundaries Simulating Walls of the Ear Canal. Sound Soft Boundary Simulating the Eardrum

The two model materials can be seen in Fig. 36, with the earplug shown in blue and the air in grey. The earplug is made from a standard silicone material with properties taken from CES Edupack.

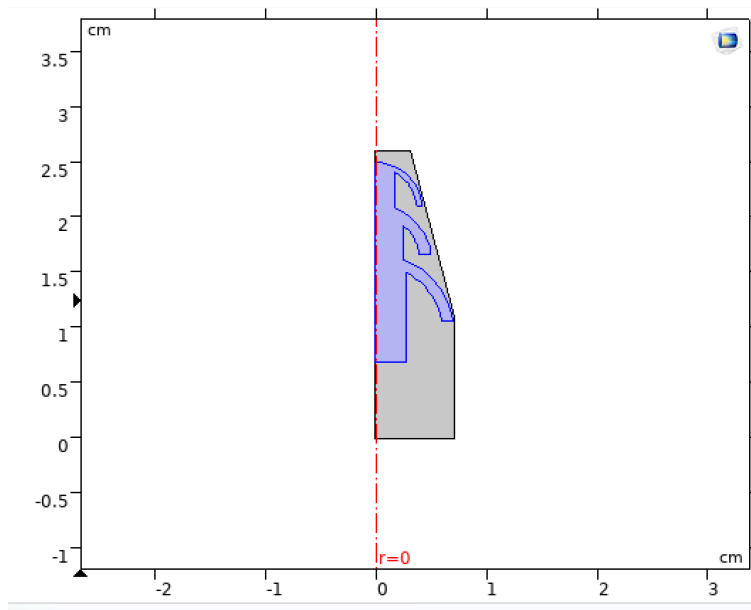


Figure 36: Triple Flange Material Domains. Earplug (shown in blue) Modeled as Silicone Material. Ear Canal Filled with Air (shown in grey)

As a result of this analysis, we hope to achieve an understanding of how the pressure waves interact with the triple flange geometry, and how attenuation varies from the porous earplug to the triple flange. Through a qualitative visual representation of the pressure in the ear canal, we also hope to determine at which stage a majority of the attenuation occurs.

4. Results

4.1 Experimental Results

Using the experimental setup that we developed, we obtained a Frequency Response Function, or FRF, of each sample. A Frequency Response Function is the relationship between the output and input of a linear system. The data that we collected was in the time domain, and we used a Fourier Transform to put the data into the frequency domain. The FRF can be used to show how well a system attenuates sound over a range of frequencies as a lower magnitude correlates to higher attenuation. We obtained a Frequency Response Function for each of the five earplugs we tested. Each earplug was tested under the same conditions using the experimental setup that we developed.

4.1.1 Porous Earplugs

Samples 1 through 3 were porous earplugs, they were dependent on their microstructure and material properties to attenuate frequencies. They each have a cylindrical shape, with two of the three including a similar tapered end. Pictures of each of these samples are shown in Fig. 37.



Figure 37: Porous Earplug Samples Used for Testing. Chosen Because of Differing Material Properties, Pore Size, and Porosity

Samples 1 and 2 are made from polyurethane foam, and Sample 3 is made from polyvinyl chloride foam. Despite the differences in material, the internal structure of each earplug is the same - small pockets of air in a moldable texture. Each of these samples attenuates frequencies well in the same range, which is between 3.5 kHz and 7 kHz. This can be seen in Fig. 38.

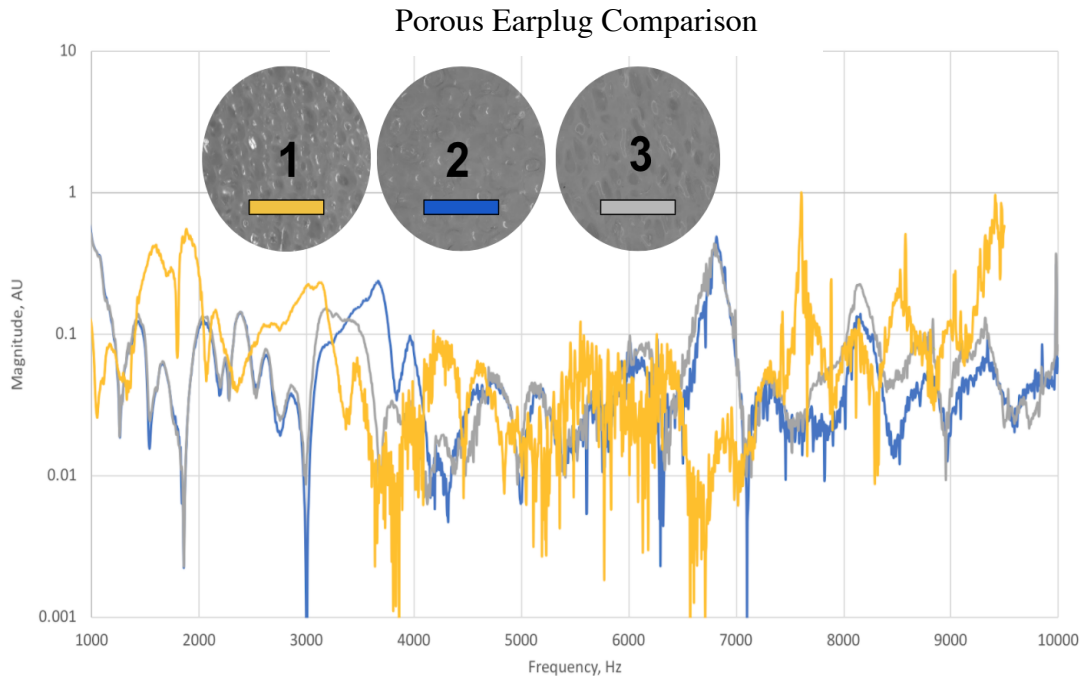


Figure 38: Porous Earplug FRF Comparison. Cross Section at 100x Magnification Shown as Representative Micro-Structure. Strong Attenuation Seen in Mid-Frequency Band with Lower Performance at Test Extremes

At the top of the graph is a picture of each of the sample's microstructures to show that they are similar, and they attenuate frequencies in the same way.

4.1.2 Non-Porous Earplugs

The other two earplugs that we tested, samples 4 and 5, were non-porous earplugs. These non-porous earplugs rely on their macrostructure to attenuate frequencies. One of the non-porous samples is made from polyurethane rubber and the other is made from a silicone wax. The

sample, shown in Fig. 39, made from polyurethane rubber has a triple-flange shape that is compressed when placed in an ear canal.



Figure 39: Representative Geometry of Triple Flange Earplug which Rely on Shape for Performance

Sample 5, however, is meant to be molded to fit into the ear canal of each user and has no particular shape. If inserted correctly, there should be no air in the ear canal. A picture of the putty, and what it looks like inserted, can be seen in Fig. 40.



Figure 40: Moldable Silicone Putty Earplug with Demonstration of Custom Insertion Properties

Sample 4 has a unique microstructure that captures air when inserted into the ear canal. Despite it being made from a relatively solid material, there is still air in the ear canal when being used. However, the silicone putty relies on completely filling the ear canal to attenuate frequencies. Sample 4 attenuates frequencies within the same range as samples 1 through 3, the porous ones, which is between 3.5 kHz and 7 kHz. The silicone putty one, however, does not attenuate in this range well at all. Instead, it attenuates better in the lower and higher frequency ranges. A comparison of the performance of samples 4 and 5 can be seen in Fig. 41.

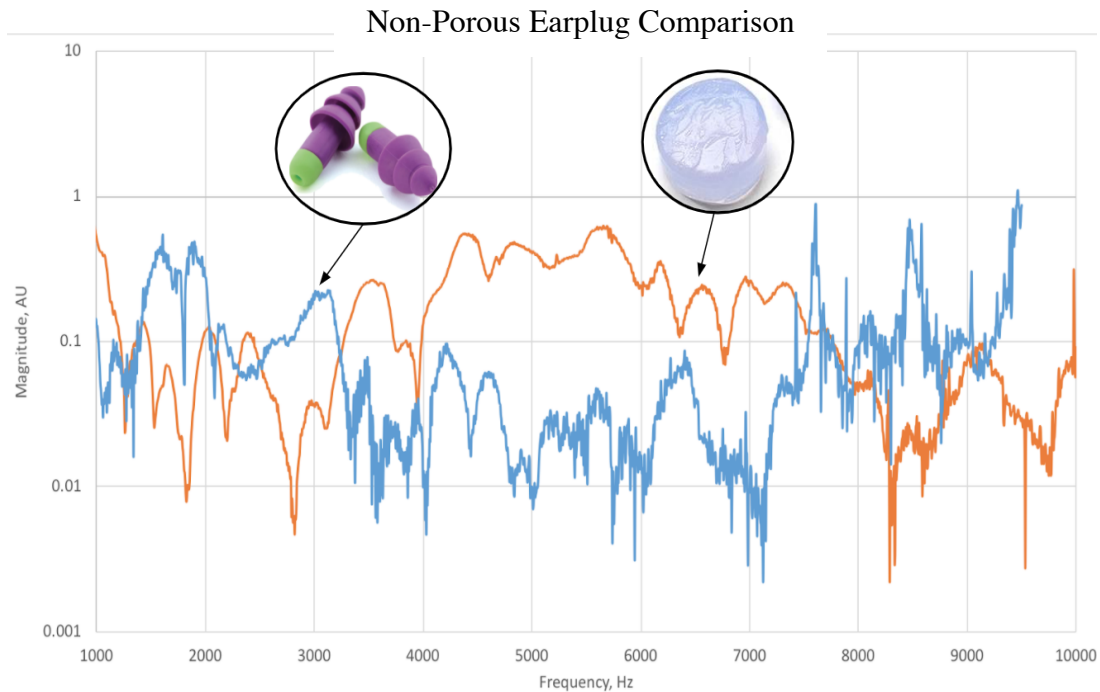


Figure 41: FRF Comparison of Non-Porous Earplugs. Though Similar Material, the Earplugs with Specialized Shape have Significant Performance Increase at Mid-Frequency Range

4.2 Microscope Characterization of Microstructure and Shape

Using the Keyence VHX 7000, images of the microstructure of each earplug sample was obtained. Five different earplugs were examined, three being classified as porous and two being classified as non-porous. In addition to this, numerical data detailing the cross-sectional values was outputted from the microscope and inputted into excel. This data was especially significant for the porous earplugs because this data allowed for the calculation of the average pore size within each plug and also used to estimate the total volume of air within the samples. An example of the results of the Keyence VHX 7000 imaging can be seen in Fig. 42.

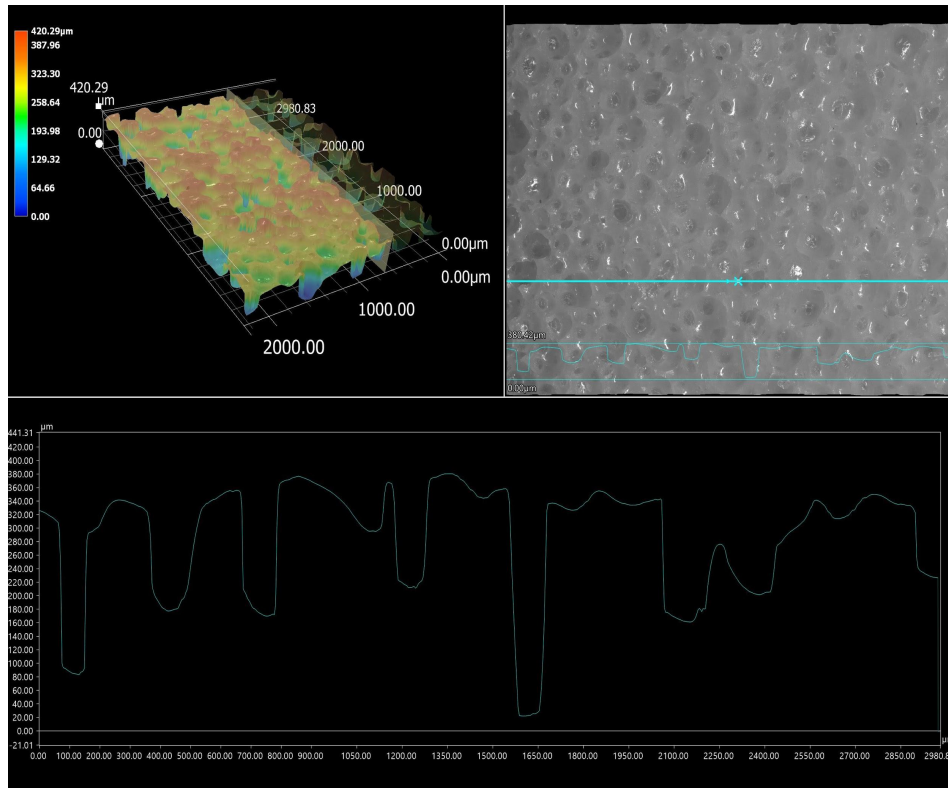


Figure 42: Sample 1 Observed Under 100x Magnification. 3D Elevation, Greyscale Image and Representative Cross-Section Graph of Elevation Shown. Quantitative Analyses Indicate an Average Pore Size of 40 [μm] and Volume of .002 [mm³]

As described, this data was used to calculate the average pore size of each porous earplug, as well as calculate the approximate total volume of air trapped within each porous earplug. The step by step calculations are outlined in Appendix E. The results of the analysis of the cross-sectional imaging and exported data to determine the average pore size of each earplug can be seen in Table 4.

Table 4: Earplug Sample Average Pore Volume

Sample	Average Pore Size
1	2,440,953.62 μm ³ = 0.002 mm ³
2	6,633,578.41 μm ³ = 0.06 mm ³
3	17,348,664.36 μm ³ = 0.017 mm ³

From the values of the average pore sizes, the total volume of air trapped within each porous earplug could be calculated. The step by step calculations for this can be found within Appendix E. The results of this analysis are presented in Table 5.

Table 5: Earplug Sample Total Volume of Air

Sample	Total Volume of Air
1	$638,328,790,860.29 \mu\text{m}^3 = 638.3 \text{ mm}^3$
2	$940,379,313,318.56 \mu\text{m}^3 = 940.4 \text{ mm}^3$
3	$1,521,985,513,125.42 \mu\text{m}^3 = 1,522 \text{ mm}^3$

Since earplugs are utilized in a compressed state, the data was also utilized to estimate the volume of within a compressed earplug. Using this value and the total air within a non-compressed earplug, a range of percent volume of air within the plug was found for each sample. These values can be seen in Table 6 and the steps to complete these calculations can be seen in Appendix E.

Table 6: Earplug Volume of Air Percentage

Sample	Percent Volume of Air
1	$22.5\% \pm 5.5\%$
2	$30\% \pm 16\%$
3	$30.5\% \pm 12.5\%$

All of these results were used to create an accurate computational model with realistic values for porosity and volume of air within the plug. The value of air in each plug was also used to compare the performance of the earplugs and act as reference values for the parametric studies conducted in COMSOL.

4.3 Computational Results

From the parametric studies on the porous earplug, we were able to determine which properties most greatly affect performance and attenuation. A 3D model was used to visualize the pressure distribution throughout the earplug. To understand the effect of parameters over our sweep, a graphical representation of $\frac{Output}{Input}$ pressure was used.

4.3.1 Porous Earplug

The earplug was modeled in COMSOL to study its response to a pressure wave. The model shown in Fig. 43 was subjected to frequencies ranging from 1,000 to 10,000 Hz and the frequency response was measured.

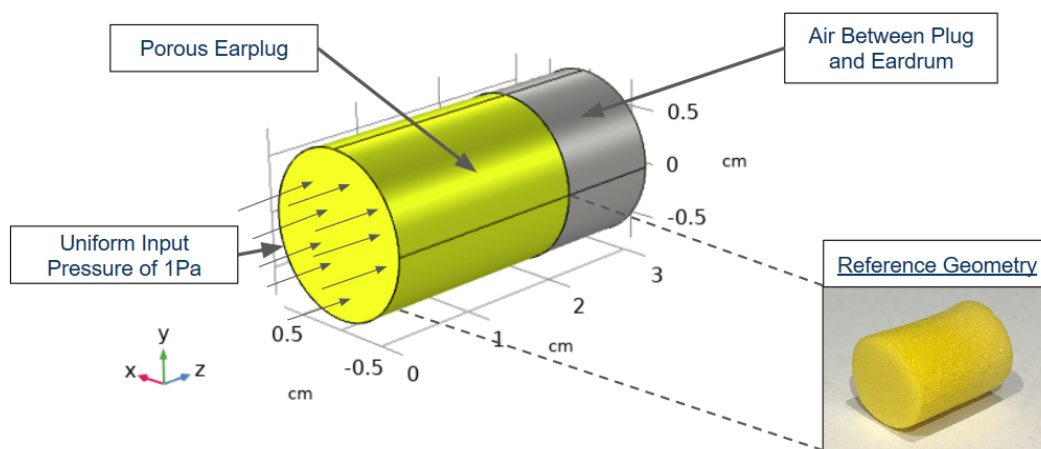


Figure 43: Porous Earplug Model in COMSOL Based on Reference Plug Geometry. Porous Earplug Shown in Yellow with Occluded Air in Grey. Model Used to Understand Performance with Varying Material Properties

Figure 44 shows a qualitative measurement of the sound pressure level distribution within the earplug and in the volume of air behind it. This shows that the geometry of the earplug is an important characteristic to consider when designing hearing protection.

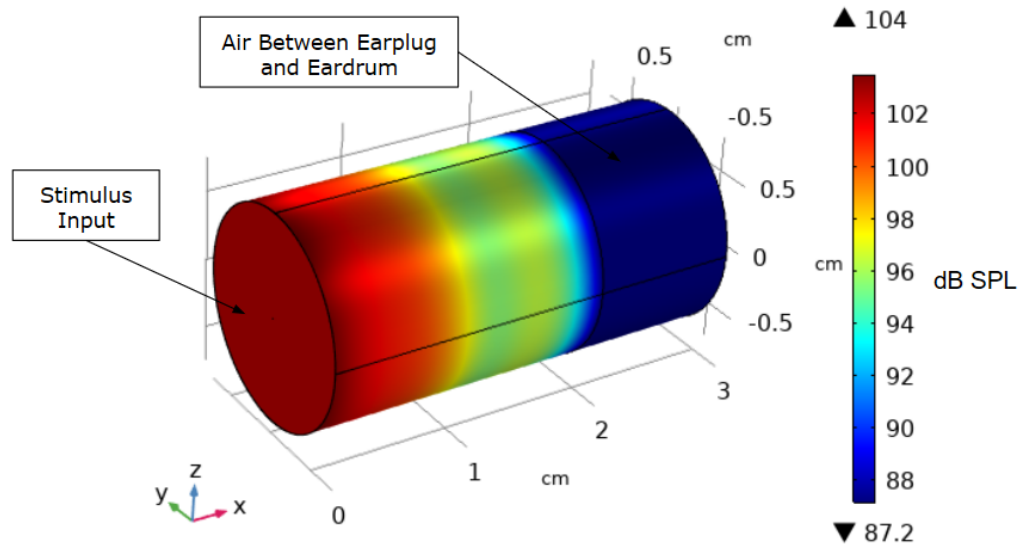


Figure 44: Sound Pressure Level Distribution in Computational Geometry at 1 kHz. Approximately 20 dB Reduction Comparable to Experimental Trials

4.3.2 Parametric Study

In addition to varying the frequency, we also ran parametric studies of six material properties at $\pm 20\%$. These were material density ρ_c , fluid density ρ_f , porosity ε_p , viscous length μ_f , shear modulus G , and Poisson's Ratio ν . We found that of these six properties, three seemed to make a significant difference in performance. These were porosity, viscous characteristic length, and fluid density.

The parametric study of porosity showed a relationship between porosity and attenuation. This is shown in Fig. 45. Porosity is defined as the proportion of air to solid in the porous material, with higher porosities having higher air content. The porosity of our tested earplugs was in the .85 - .93 range. From our computational tests, we see that the porosity of the earplug has a direct impact on the attenuation of sound where higher porosities attenuate more sound. This is the case for all frequencies in the 1,000 to 10,000 Hz range. Porosity seems to have a particularly large effect at higher frequencies, with the lower porosities attenuating significantly worse than the higher.

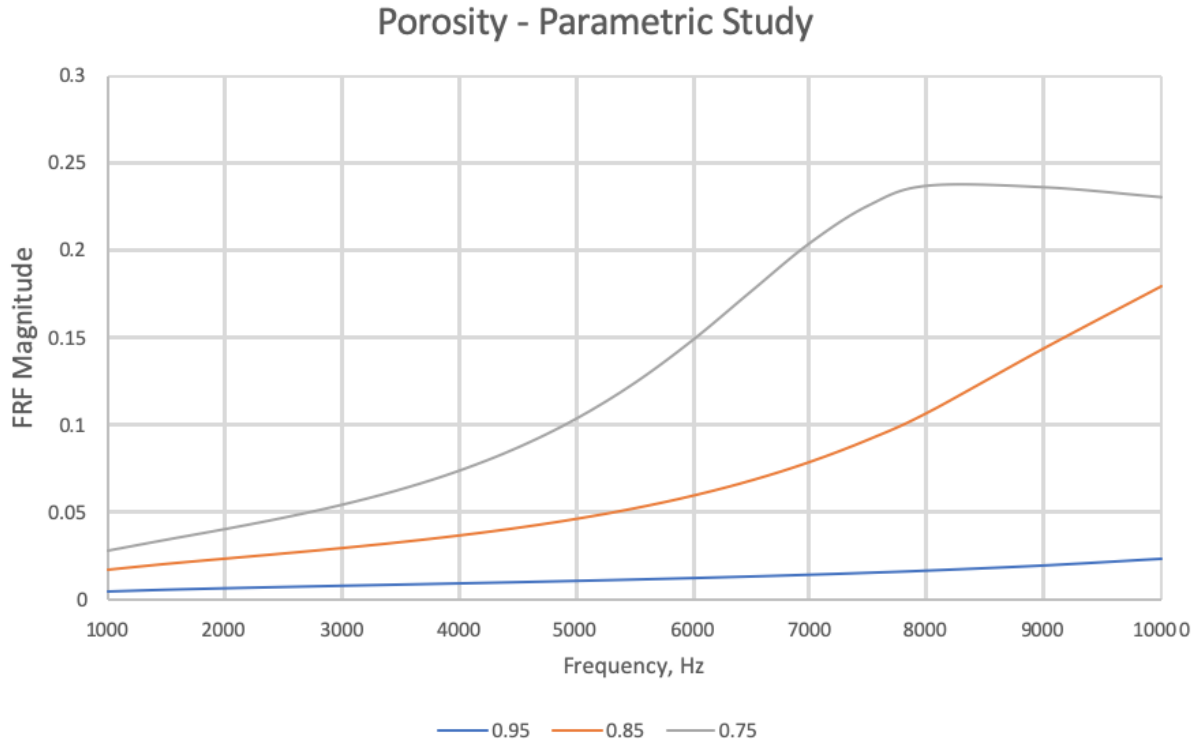


Figure 45: Results of Porosity Parametric Study at Values of .75, .85 and .95 from 1 - 10 kHz Showing as Porosity Decreases (volume of air decreases), Attenuation is Reduced, Especially at Higher Frequencies

The parametric study of viscous characteristic length showed a relationship between viscous characteristic length and attenuation and can be seen in Fig. 46. Viscous characteristic length is defined as the mean distance between pore walls, or pore diameter for a spherical pore. From this analysis, we see that a smaller pore size absorbs more acoustical energy. Having smaller pores creates more interactions and reflections between the incoming acoustical wave and the solid matrix material, in turn dissipating more energy. The difference in attenuation becoming larger at higher frequencies is also as expected because as the wavelength decreases, the pore size on the micrometer scale has a larger effect.

Viscous Characteristic Length - Parametric Study

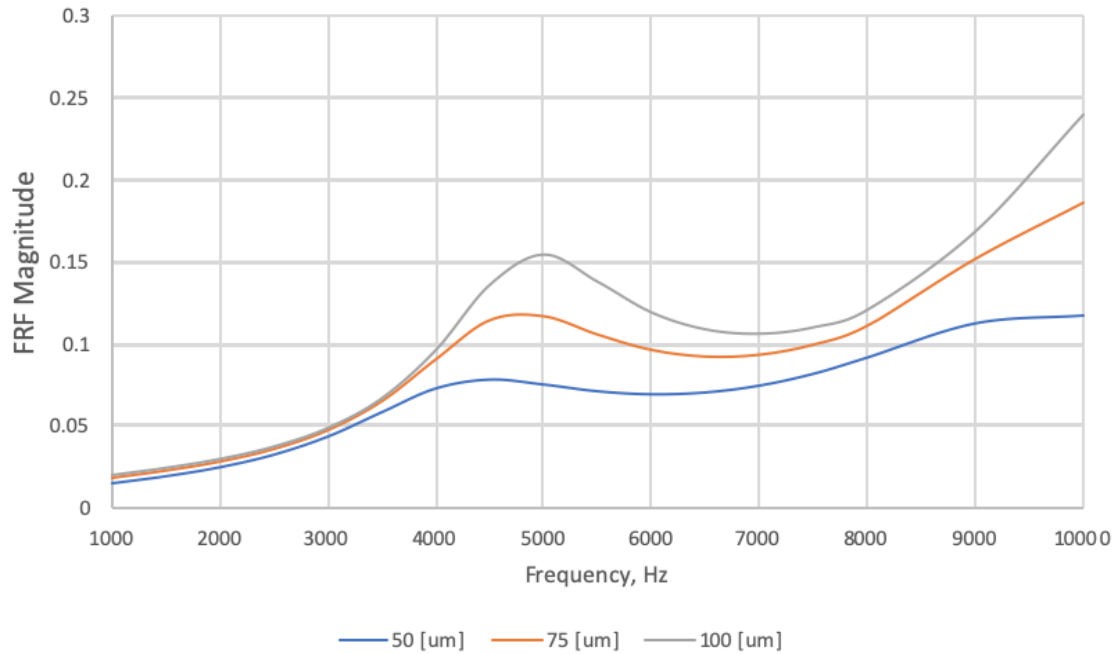


Figure 46: Results of Viscous Length Parametric Study at Values of 50, 75 and 100[um] from 1 - 10 kHz. Results Indicate a Smaller Viscous Length is Linked to Greater Earplug Performance

The final parameter that largely affected attenuation was the fluid matrix density. This is the density of the fluid component in a porous material, which in our case is air. One interesting observation was made from studying Fig. 47. As the fluid density matrix increases, the function shifts to the left. This is an important relationship because this parameter will allow for control of which frequencies are dampened and which are let through.

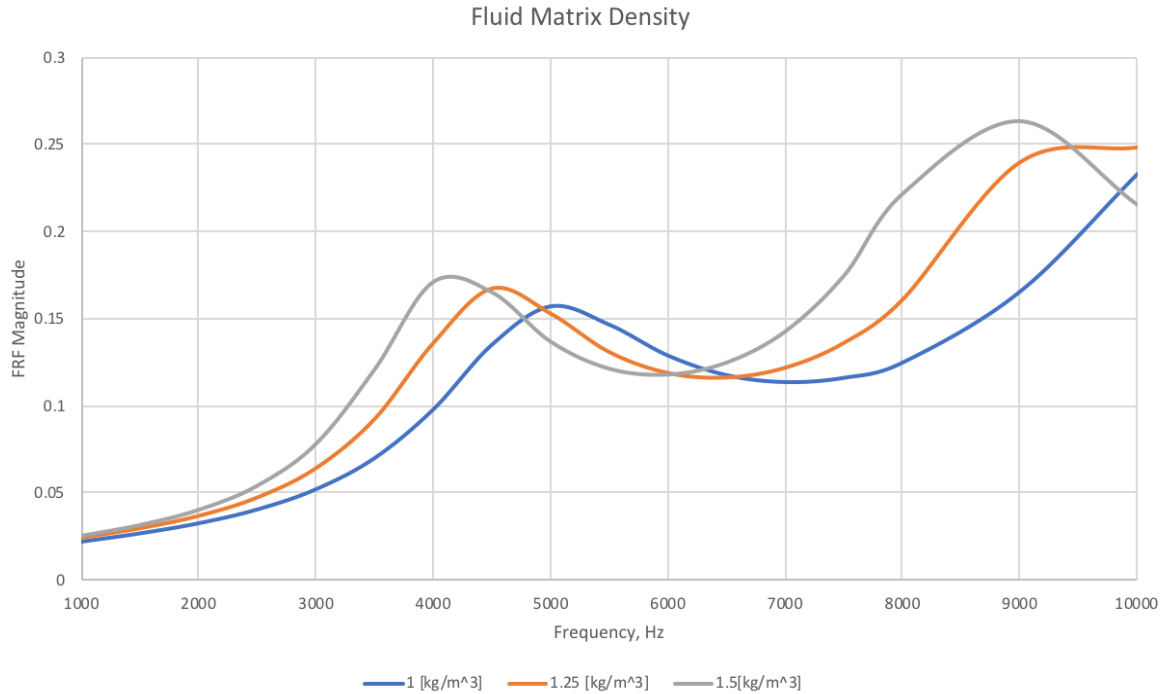


Figure 47: Results of Fluid Matrix Density Parametric Study at Values of 1, 1.25 and 1.5 [kg/m³] from 1 - 10 kHz. Lower Fluid Density Shifts FRF Peaks Towards the Right

4.3.3 Triple Flange Earplug

A computational analysis was also performed on the triple flange to understand qualitatively how the flanges interact with an incoming pressure wave. To reduce computational time, the earplug was modeled as a 2D axisymmetric geometry. The 3D representation is the rotation of this geometry 180 degrees. From this visual, we see that each flange acts as a barrier with pressure dropping at each interval. A majority of the attenuation seems to come from the smaller two flanges after the initial front is broken by the largest flange. Overall, it seems that the more flanges there are, the higher attenuation can be expected. We can confirm relative accuracy as the triple flange earplug had a comparable decibel drop-in testing as seen in the computational model. Additionally, as we predicted, the triple flange earplug attenuated sound on the same magnitude of the porous earplug, showing the volume of occluded air as an important property in both cases. Representative results are shown in Fig. 48, which correspond to the computed acoustical pressure across a cross-section of the triple flange plug.

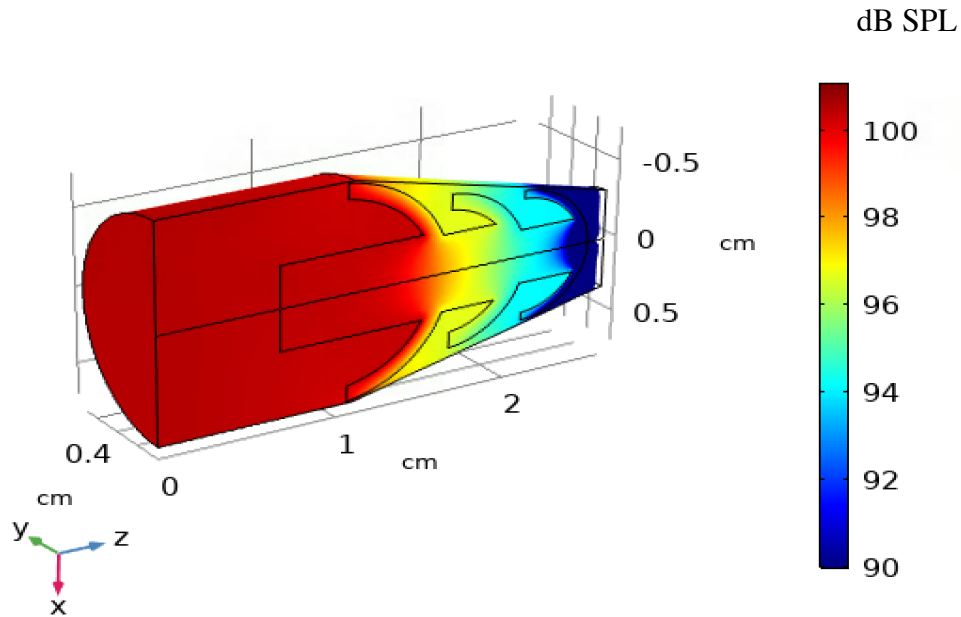


Figure 48: Cross-sectional Triple Flange Pressure Distribution. Results Show a Pressure Reduction at Each Flange, with Overall Attenuation in a Similar Range to Porous Plugs

One limitation of this model is the inability to compress the triple flange material. In actual application, these flanges would be compressed varying amounts by the geometries of individual ear canals, and this would likely have an effect on attenuation. This study can be used in conjunction with new manufacturing technologies such as 3D printing to design and realize structures that were not previously possible.

5. Discussion

5.1 Microstructure, Macrostructure, and Performance

Through analytical, experimental, and computational work, our team learned that porosity is the material property with the biggest impact on attenuating sound. The correlation between microstructure, macrostructure and attenuation is strong and enables future engineers to consider this when working on innovative new hearing protection devices. A visual representation of this relationship is shown in Fig. 49. The results of the parametric study on porosity, supplemented with experimental data, showed a positive correlation.

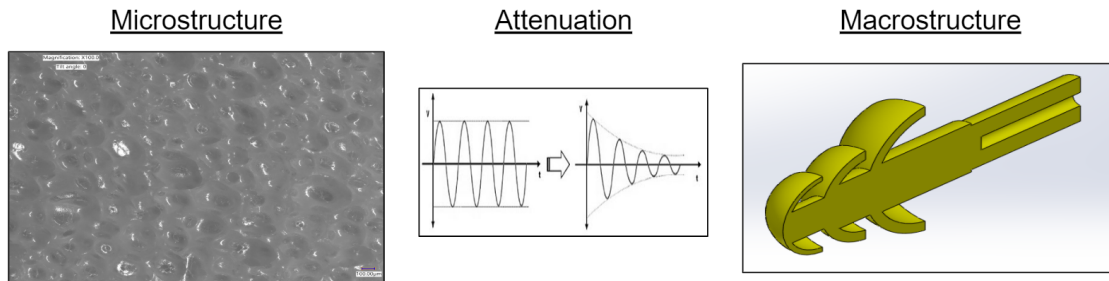


Figure 49: Our Process Considered Microstructure along with Macro Structure to Understand the Effect on Overall Attenuation

5.2 Developing the Correlation

The microstructure was found to be the most important aspect of earplug attenuation, but through our work, we also found a strong correlation between shape, or macrostructure, and attenuation. The computational model showed that porosity and fluid matrix density had a strong influence on the frequency response function. Porosity allowed for the control of attenuation over all frequencies while fluid matrix density allowed for the control of which frequencies are attenuated. The results from the computational model were backed up by our experimental testing. In the experimental testing we saw a large increase in attenuation when comparing several of the porous samples to the non-porous sample. The majority of the attenuation differences were seen in the 4-7 kHz range. This was thought to be a result of our experimental fixture actually damping some of the frequencies passing through the aperture in the Pinna Fixture. This was confirmed by running the same experiment with no earplug samples and the result was an FRF of the fixture that showed its damping characteristics at low frequency ranges. From both the experimental and computational models we are able to derive a direct correlation between porosity and attenuation. In Fig. 50 the correlation can be seen while also seeing the difference in microstructure.

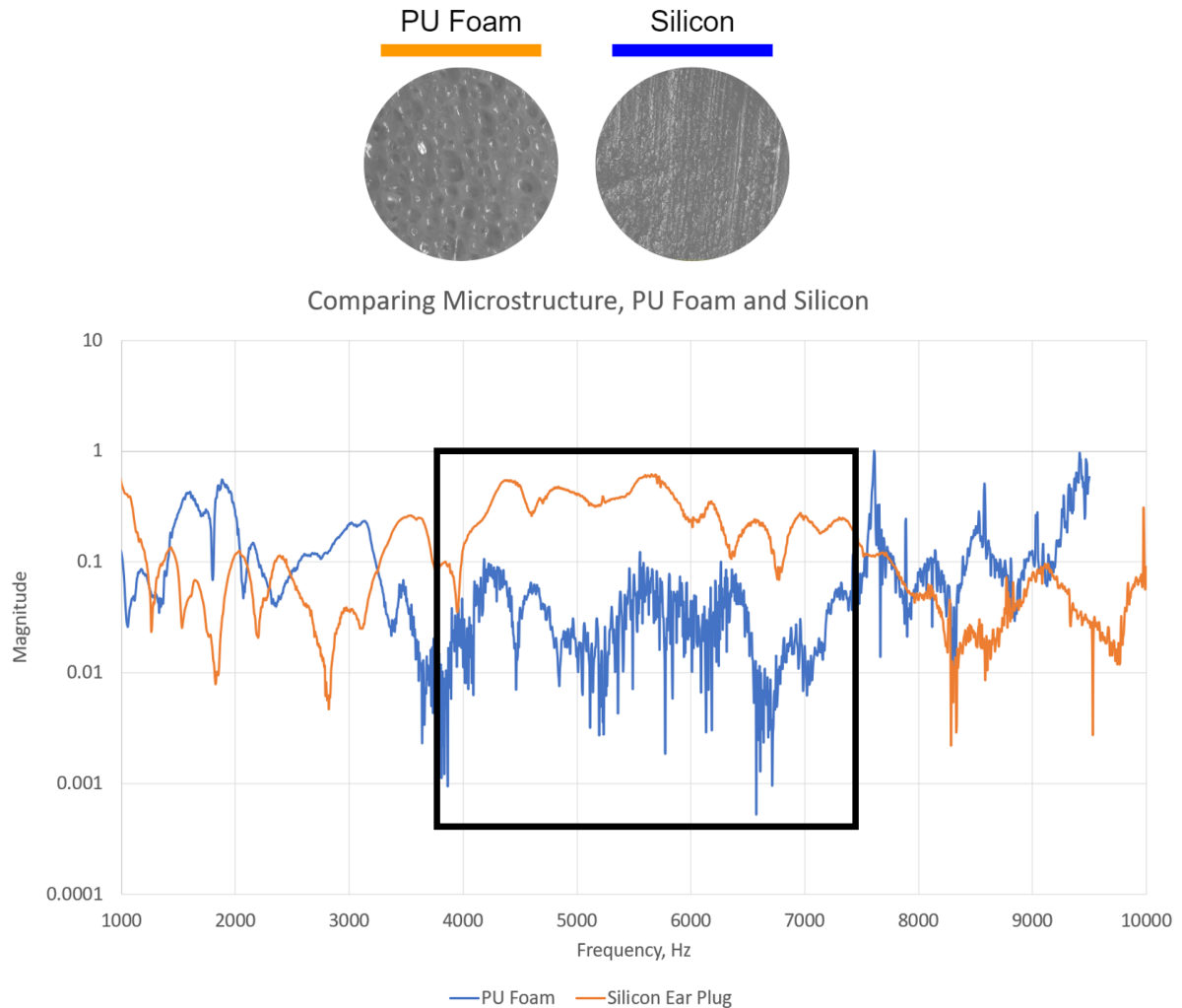


Figure 50: Microstructure and Performance Between Porous and Non-Porous Samples. The FRF Compares Samples with Dramatically Different Micro-Structures that Share Similar Shape

The two non-porous samples that we tested had very different physical shapes, yet both materials had negligible porosity. However, they attenuated sounds very differently. The triple-flange earplug attenuated sound much better due to its shape than trapped air. From the similarities in their microstructure, but differences in their macrostructure, we can draw a correlation between the macrostructure and frequency attenuation. This finding was supported even further with the parametric study on triple flange shapes in our COMSOL model. It was concluded that one of the most important factors of the porosity of the earplugs is the amount of air that is inside each sample. The more porous samples naturally have more air volume inside of them. Our work characterized the performance of the triple flange earplug in a similar way. It was found that the flanges each trap a volume of air when inserted into the ear canal. These pockets of air actively damp many frequencies that we tested for and allowed the triple flange earplug to attenuate

comparatively to the porous materials. In the future, more research on the different shapes that earplugs take could prove to be very influential in attenuation and innovative earplug design.

5.3 Application to Additive Manufacturing

With an understanding of the correlation we found and our experimental setup, future engineers will be able to further characterize earplug shape and the role it plays in attenuating damaging frequencies. In addition, this research could pave the way for advances in metamaterials.

Recently there has been great interest in the development of these metamaterials because of their ability to be engineered in unique ways that refract and or dampen light, sound and electromagnetic radiation. Metamaterials could be applied to acoustics to guide the trajectory of frequencies entering the earplug and ultimately attenuate harmful noises. Utilizing innovative rapid prototyping processes, engineers will be able to develop advanced macrostructures of materials while also engineering the proper microstructure mechanics to protect the ear from a variety of high-intensity frequencies. Future engineers can also use our parametric analyses to begin constructing composite materials with varying densities and porosities to achieve their desired result.

6. Conclusions and Recommendations

Through our research, we've found the importance of porosity in attenuating sound waves. In addition, we've developed methodologies to verify the attenuation levels of earplugs prior to manufacturing. With these systems and new additive manufacturing, engineers will be able to design earplugs that attenuate specific frequencies. New technologies will incorporate varying levels of porosity for functionality across a spectrum of damaging noises.

We recommend additional validation prior to using these methodologies. We did not perform tests on multiple samples of the same earplug. This would validate the Frequency Response Functions that we created by using the average of multiple samples. In addition, we recommend creating preliminary composite materials by testing two earplugs of different materials at the same time. The results from our computational and experimental work identified the prospect of utilizing these composite earplugs for improved attenuation of higher frequency sounds while still letting through the lower, less damaging frequencies such as verbal commands. Further investigation of composite materials or varying porosity within a single earplug will create the opportunity to achieve better attenuation. These new technologies can be utilized to preserve the hearing system in work and recreational activities.

6.1 Difficulties Driven by COVID-19

COVID-19 has affected almost every aspect of the world, and our project is no different. We had plans to continue to gather data, refine our computational model, and validate the work that we had done. However, without the access to our lab, gathering data to validate our work was impossible. Almost seven months into our project we had to adapt to working as a team while we weren't physically together. Each team member had to cope with the adjustment of taking classes from home, the changes that were happening with the end of our college career and the beginning of our professional careers. Despite the challenges that we faced; we developed a methodology that will assist in creating more effective hearing protection devices.

7. Future Work

7.1 Apply to a Nonlinear System: Shock Tube

From applying the earplugs to a linear sound wave, we learned the importance of porosity, and the way earplugs react to long sustained noises. As mentioned previously, individuals are subjected to a variety of noises which are represented by different sound waves. In order to create a complete earplug, understanding how earplugs react to nonlinear sound waves is important. These nonlinear sound waves can be created through the shock tube that was designed and manufactured by a previous MQP team. Our experimental setup was designed for the use of the shock tube.

Our team was unable to apply our system with the shock tube due to the unforeseen complications, yet the first step of future work should include using the same experimental setup and procedure to subject the same samples to impulse blasts. This shock wave produces a very intense and broad frequency range. The non-linear sound waves will make the earplugs react differently than the linear input in the Frequency Sweep Experiment. Using the system, we developed, an FRF can be obtained using the blast data. This experiment would have given us an even greater understanding of the relationships between microstructure, macrostructure, and performance. This information will be very helpful for the future design of level-dependent hearing protection.

7.2 High-Speed Imaging

In the system that we adapted, there is access to a Schlieren FASTCAM SA5 camera. During the creation of the anechoic chamber, we took into consideration the imaging techniques that could be used in the future. Because of this, the chamber has removable sides, so the laser is able to reflect off of the parabolic mirror that is used for imaging. Diagrams of the experimental setup to accommodate the Schlieren imaging is presented in Fig. 51 and 52.

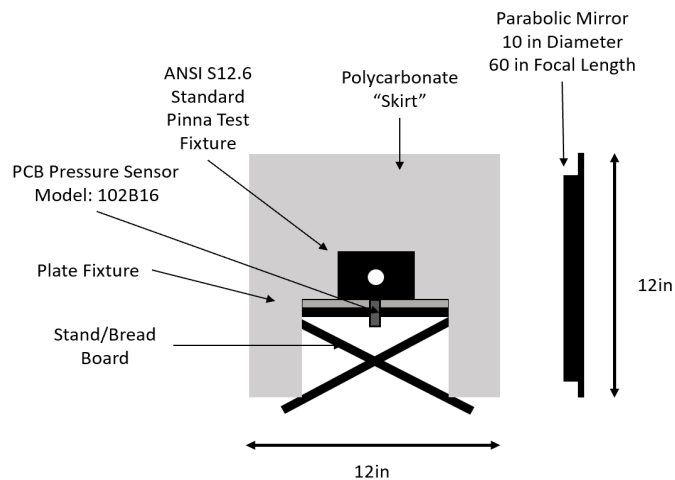


Figure 51: Diagram of Experimental Setup Viewed from the Output of the Shock Tube. Skirt Blocks Approaching Wave from Exciting Back Sensor

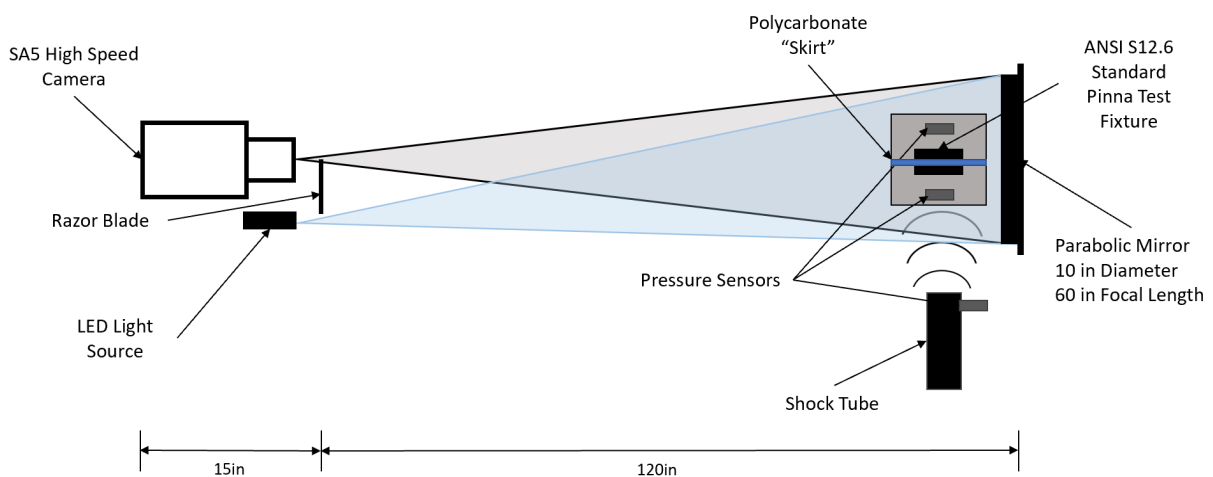


Figure 52: Diagram of Aerial View of Experimental Setup Including the High-Speed Camera and Mirror Used for Schlieren Imaging. Setup Allows Pressure Readings to be Correlated with Video

We suggest utilizing the imaging system when applying impulse blasts to the hearing protection devices. With this imaging, the attenuation levels of the hearing protection devices will be visual. The team did some preliminary imaging of a high-speed shock shown in Fig. 53.

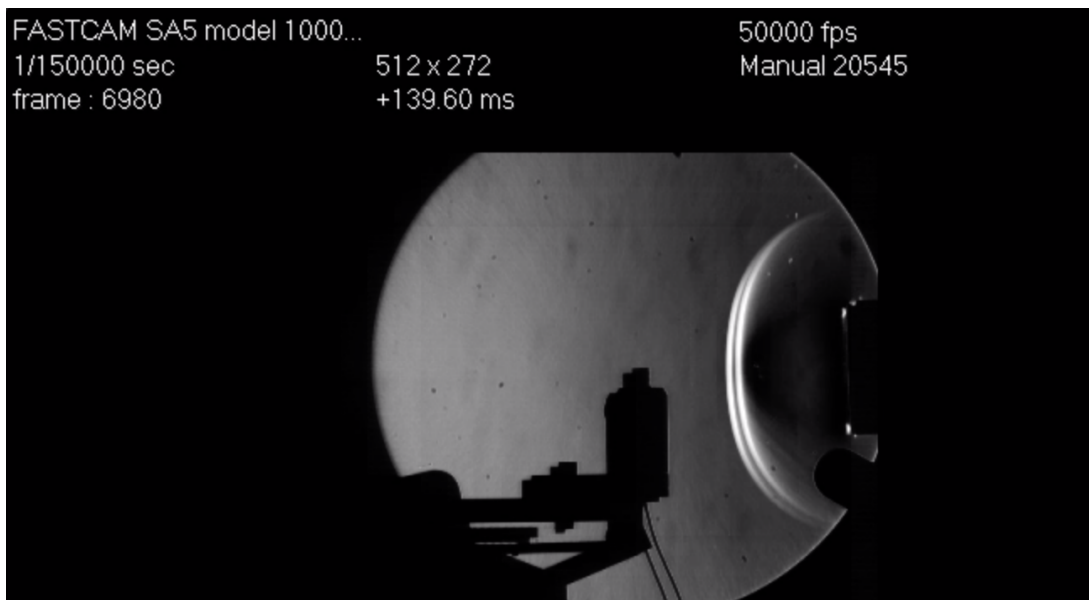


Figure 53: Image Captured Using the High-Speed Camera and Schlieren Technique. High Pressure Wave Front Seen Leaving Shock Tube Mouth Traveling Towards Pressure Sensor

7.3 Using Computational Model to Make Design Recommendations

The computational model that we developed allows for changes in different material properties and different ratios of composite materials. Our third and final recommendation is to validate and use the computational model that we developed to design different materials for specified frequency attenuation. Different materials, geometries, and configurations can be input into the model easily which can provide preliminary results without experimental investigation. Once the earplug is created, it can be tested for real-world applications using the experimental setup that we designed.

With the addition of the recommendations that we made; we are confident that our methodologies will be able to assist future engineers in the creation of more efficient passive hearing protection devices.

References

- [1] Noise-Induced Hearing Loss. (2019, June 14). from <https://www.nidcd.nih.gov/health/noise-induced-hearing-loss>.
- [2] Gerges, S. N. Y., & Vedsmand, L. (n.d.). PERSONAL MEASURES AND HEARING CONSERVATION. from https://www.who.int/occupational_health/publications/noise11.pdf.
- [3] How Do We Hear? (2018, January 3). from <https://www.nidcd.nih.gov/health/how-do-we-hear>.
- [4] Gorman, Benjamin. (2018). A Framework for Speechreading Acquisition Tools.
- [5] Geisler, C. D. (1998). From Sound to Synapse: Physiology of the Mammalian Ear. New York: Oxford University Press, pp. 14-291.
- [6] Packer, L. & Ohio University. (2015, April 2). Ears: They are smarter than you think. from <https://www.healthyhearing.com/report/52419-Ears-they-re-smarter-than-you-think>.
- [7] Acoustic Reflex. (n.d.). from <https://www.sciencedirect.com/topics/medicine-and-dentistry/acoustic-reflex>.
- [8] Sound Waves as Pressure Waves. (2017). from <https://www.physicsclassroom.com/class/sound/u1l11c.cfm>.
- [9] Introduction to Sound Waves. (n.d.) from <https://studyonline.zohosites.com/Sound-Waves.html>.
- [10] National Research Council (US) Committee on Disability Determination for Individuals with Hearing Impairments. (1970, January 1). Basics of Sound, the Ear, and Hearing. from <https://www.ncbi.nlm.nih.gov/books/NBK207834/>.
- [11] Griffiths, G. W., & Schiesser, W. E. (n.d.). Linear and nonlinear waves. from http://www.scholarpedia.org/article/Linear_and_nonlinear_waves#Linear_waves.
- [12] Sound Intensity and Sound Level. (n.d.). from <https://courses.lumenlearning.com/physics/chapter/17-3-sound-intensity-and-sound-level/>.
- [13] Berg, R. E. (2020, April 6). Steady-state waves. from <https://www.britannica.com/science/sound-physics/Steady-state-waves#ref64005>.

- [14] Waisman, Federico & Gurley, Kurtis & Grigoriu, Mircea & Kareem, Ahsan. (2002). Non-Gaussian Model for Ringing Phenomena in Offshore Structures. *Journal of Engineering Mechanics-asce - J ENG MECH-ASCE*. 128. 10.1061/(ASCE)0733-9399(2002)128:7(730).
- [15] What is a Frequency Response Function (FRF)? (2019, August 29). from <https://community.sw.siemens.com/s/article/what-is-a-frequency-response-function-frf>.
- [16] What Noises Cause Hearing Loss? | NCEH | CDC. (n.d.). from https://www.cdc.gov/nceh/hearing_loss/what_noises_cause_hearing_loss.html.
- [17] Sengpiel, E. (n.d.). Damping of Sound Level (Decibel dB) vs. Distance. from <http://www.sengpielaudio.com/calculator-distance.htm>.
- [18] “Why Do We Need to Hear?” Hearing Link, July 2, 2019. <https://www.hearinglink.org/your-hearing/about-hearing/why-do-we-need-to-hear/>.
- [19] Brown, Andrew D., et al. “Effects of Active and Passive Hearing Protection Devices on Sound, Source Localization, Speech Recognition, and Tone Detection.” *PLOS ONE*, Public Library of Science, journals.plos.org/plosone/article?id=10.1371%2Fjournal.pone.0136568.
- [20] CirgenskiMay, Tabatha. “How to Choose the Most Effective Hearing Protection?” *Occupational Health & Safety*. From <https://ohsonline.com/Articles/2017/05/01/How-to-Choose-the-Most-Effective-Hearing-Protection.aspx>.
- [21] Buck, K. “Active Hearing Protection Systems and Their Performance”. French-German Research Institute. (2019).
From <https://pdfs.semanticscholar.org/f449/75bd14335870ee8f929bd834cdca1598676d.pdf>
- [22] Sep 01, 2017. “New ANR Technology in Triple Hearing Protection Safely Extends Work Time.” *Occupational Health & Safety*. Accessed May 17, 2020. <https://ohsonline.com/Articles/2017/09/01/New-ANR-Technology-in-Triple-Hearing-Protection.aspx?Page=2>
- [23] Gallagher, H. “Performance Assessment of Passive Hearing Protection Devices”. Air Force Research Laboratory. (2014). From <https://apps.dtic.mil/dtic/tr/fulltext/u2/a615393.pdf>.
- [24] “Earplug & Noise Reduction Ratings Explained.” *Magento Commerce*. Accessed May 16, 2020. From <https://www.coopersafety.com/earplugs-noise-reduction>.
- [25] Staff, H. R. (2014, February 28). *Hearing Protection Devices: Current Standards and Pending...* from <https://www.hearingreview.com/hearing-products/hearing-protection-devices-current-standards-and-pending-development>.

- [26] Biabani, A., Aliabadi, M., Golmohammadi, R., & Farhadian, M. (2017). Individual Fit Testing of Hearing Protection Devices Based on Microphone in Real Ear. *Safety and health at work*, 8(4), 364–370. <https://doi.org/10.1016/j.shaw.2017.03.005>
- [27] Attenuation of Sound Waves. From <https://www.nde-ed.org/EducationResources/CommunityCollege/Ultrasonics/Physics/attenuation.htm>.
- [28] Zhang, Yi, "Measuring Acoustic Attenuation of Polymer Materials Using Drop Ball Test" (2013). *Dissertations and Theses*. 151. <https://commons.erau.edu/edt/151>.
- [29] Frank, E. W., Roberge, J. Y., Walsh, J. C., & Perkoski, J. J. (2019, June 15). Digital WPI. from <https://digitalcommons.wpi.edu/mqp-all/7128/>.
- [30] ANSI/ASA S12.6-216, American National Standard Methods for Measuring the Real-Ear Attenuation of Hearing Protectors, New York, 2016.
- [31] Lecture 11 The Fourier Transform. (n.d.) From <https://web.stanford.edu/class/ee102/lectures/fourtran>.
- [32] COMSOL Multiphysics®, 2018, v. 5.4. www.comsol.com. COMSOL AB, Stockholm, Sweden
- [33] Introduction to Acoustics. (2018, June 11). from <https://www.comsol.com/multiphysics/acoustics>.

Appendices

Appendix A: Safety Protocol

An analysis on all of the ways the Frequency Sweep Experiment could cause harm to the researchers or the lab.

Experimental Procedure

- The Frequency Sweep Experiment was created in order to test the attenuation levels of different passive hearing protection devices. An experimental setup has been developed in order to best isolate the sound waves for an accurate reading of how the passive hearing protection device attenuates sound. Using a LabVIEW code that we developed, a Frequency Response Function is created to visualize how well each sample attenuates sound.

Potential Hazards:

- High frequency noises could be heard
 - Each researcher in the room should be wearing hearing protection devices. If earmuffs are not sufficient, double up on hearing protection and wear earplugs in addition to the earmuffs.
 - Notify those in neighboring spaces that the experiment is being conducted to ensure those around do not expose themselves to damaging frequencies.
 - Ensure that the experiment is being done in a closed space to avoid sound waves traveling.
 - Put on the side of the anechoic chamber. Be sure to secure sides down with clasps.
- High-speed imaging is being utilized therefore the anechoic chamber cannot be closed.
 - Each researcher in the room must double up on hearing protection. Use earmuffs in addition to earplugs.

Appendix B: Frequency Sweep Operating Procedure

LabVIEW

1. Turn on DAQ and open up the FRF Test LabVIEW program.
2. Connect two microphones to BNC adapters.
3. Plug each BNC into DAQ inputs and insert those designations into LabVIEW software.
4. Set the samples per channel to 10,000.
5. Set the sampling rate to 50,000.
6. Set the averaging to 100 averages.
7. Run the program to test microphone responses.

Experiment Procedure

1. Output frequency sweep stimulus from frequency generator to speaker.
2. Test LabVIEW to see if microphones are outputting single frequency by outputting a single frequency from the speaker and analyze the graphs on LabVIEW.
3. After the sweep is being output into the experimental chamber run the LabVIEW software with the stimulus on repeat until the program is done averaging.
4. To save this data, write out the plots to an excel file (97 Workbook file).
5. Analyze the FRF graph in excel.
6. Repeat for multiple samples.

Appendix C: LabVIEW Code for Frequency Sweep Experiment

The complete LabVIEW code used for our frequency sweep experiment can be seen in Fig. C1. This program takes the input from two analog ports, displays the raw data from both on the front panel along with the Fourier transformations of each.

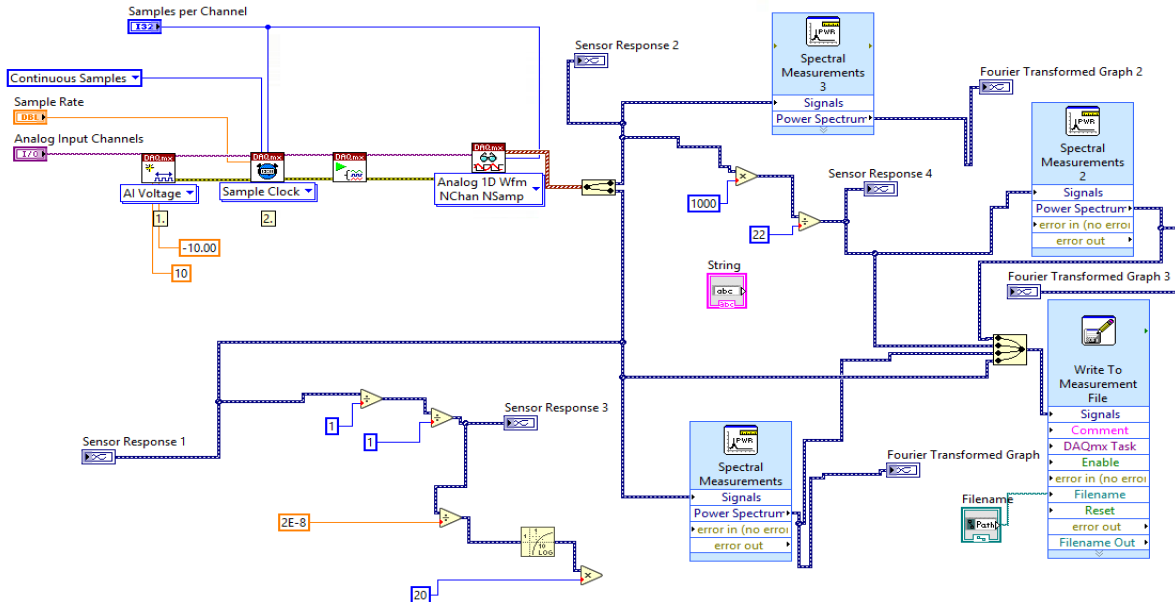


Figure C1: Overview of LabVIEW Program to Read Raw and Transformed Data from Two Sensors

Fig. C2 shows the construction of two analog input channels for the LabVIEW code. In this part of the code we added sampling rate, samples per channel and the input voltages from the DAQ. These can be modified by the user on the front panel.

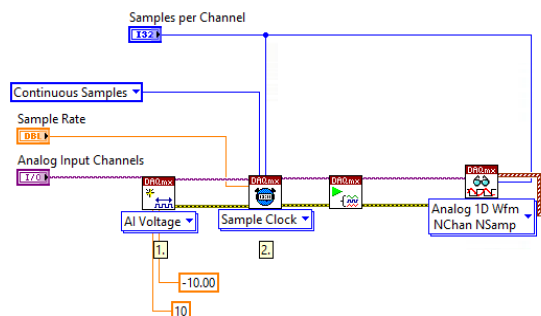


Figure C2: Initialization of Two Input Channels

Each channel is split into a raw and transformed component, shown in Fig. C3. LabVIEW provides a spectral measurements module that automatically takes the Fourier transform of an input signal. The calibration values are applied to convert input voltage to pressure.

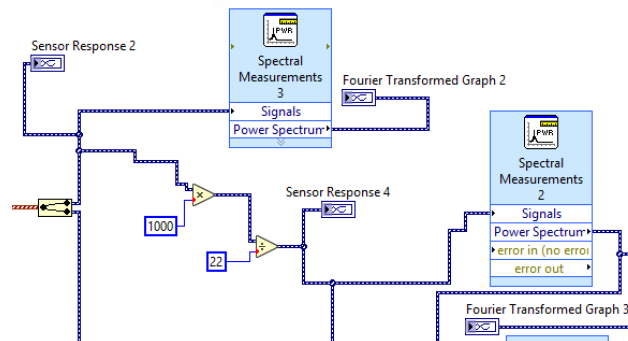


Figure C3: Conversion of Input Data to Calibrated Pressure and Fourier Transformed Data

These FFTs and calibrated pressures are displayed as graphs on the front panel so that we can constantly monitor individual responses from each microphone. These are also written out to an Excel file so that the raw data along with the transformed data can be saved. Fig. C4 shows the saving process.

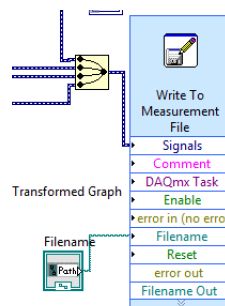


Figure C4: Process to Export LabVIEW Output to Excel Document

The top panel in Fig. C5 allows for modification of sampling rate, samples per channel, input channels and output file. As described earlier, the front panel displays the various information recorded for constant monitoring. The left column of graphs displays the raw response in voltage while the right column displays the FFT. These are helpful to verify the expected response during an experiment.

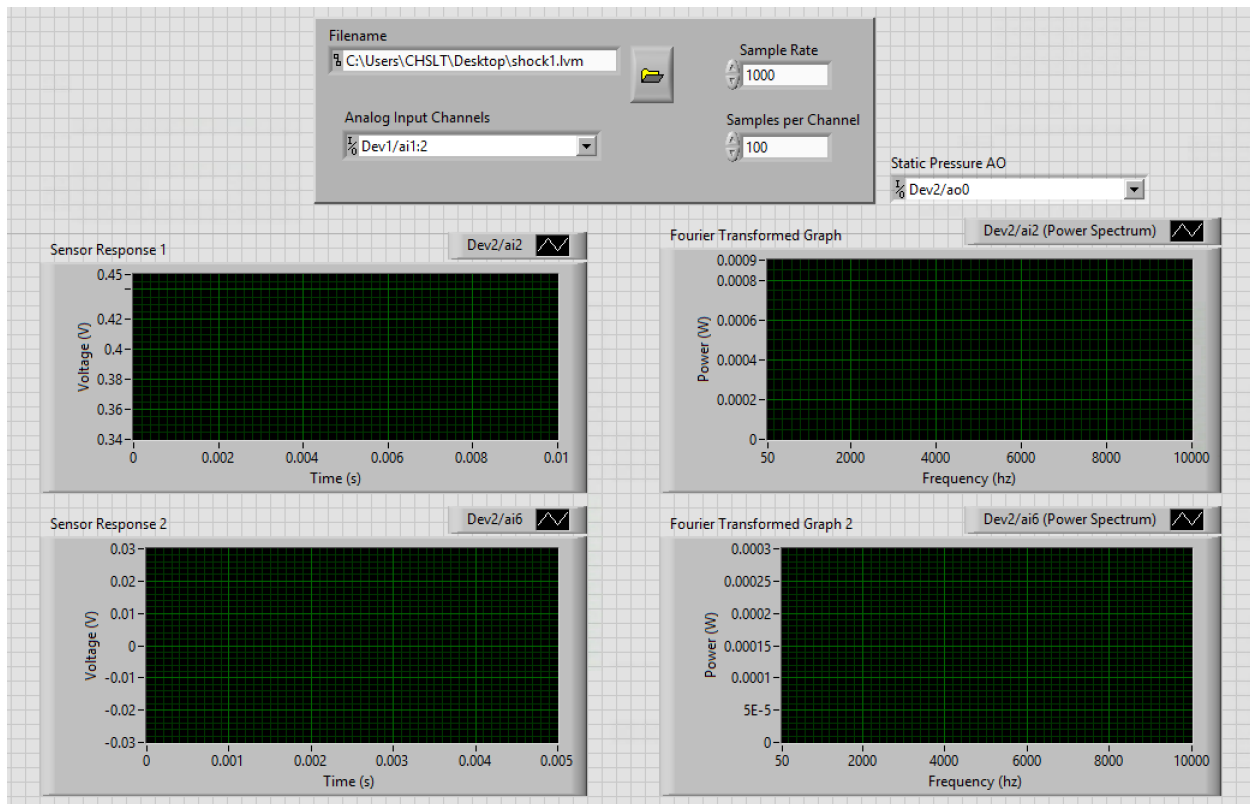


Figure C5: Front Panel of LabVIEW with Input Parameters and Monitoring Graphs

Appendix D: Frequency Sweep Experimental Setup Diagrams

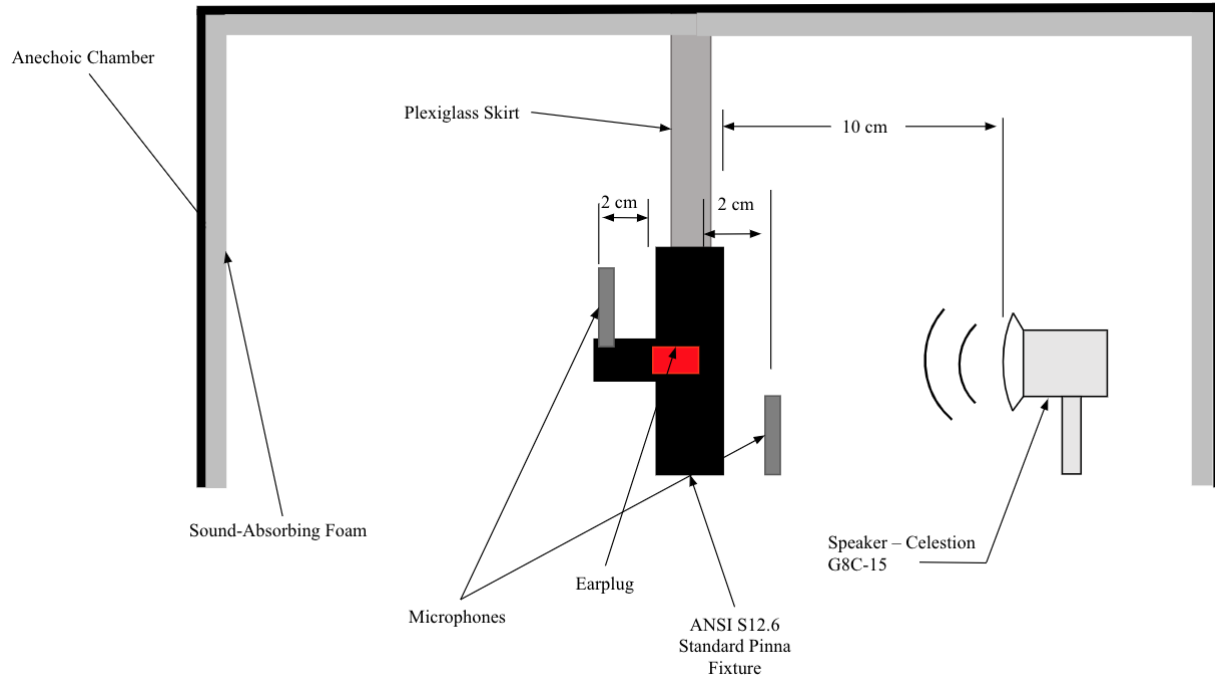


Figure D1: Diagram of Frequency Sweep Experiment

Figure D1 depicts a diagram of the setup for the frequency sweep experiment. Shown in black is the ANSI S12.6 fixture that the team manufactured. The fixture should be sitting on top of the manufacturing plate on the adjustable platform. The earplug, shown in red, should be inserted into the through hole of the fixture as it would be inserted into an ear canal. The microphones should be placed two centimeters from the front and back of the earplug. The Celestion G8C-15 speaker should be placed ten centimeters from the front of the ANSI S12.6 fixture. Placed over the fixture is the sound barrier that the team manufactured. The side of the sound barrier that is covered with sound-absorbing foam should be facing the sound source. Each element mentioned thus far should be surrounded by the anechoic chamber lined with sound-absorbing foam. Prior to testing, be sure to clasp the sides of the anechoic chamber in place. Figure D2 shows the electrical schematic that is necessary to complete the Frequency Sweep Experiment.

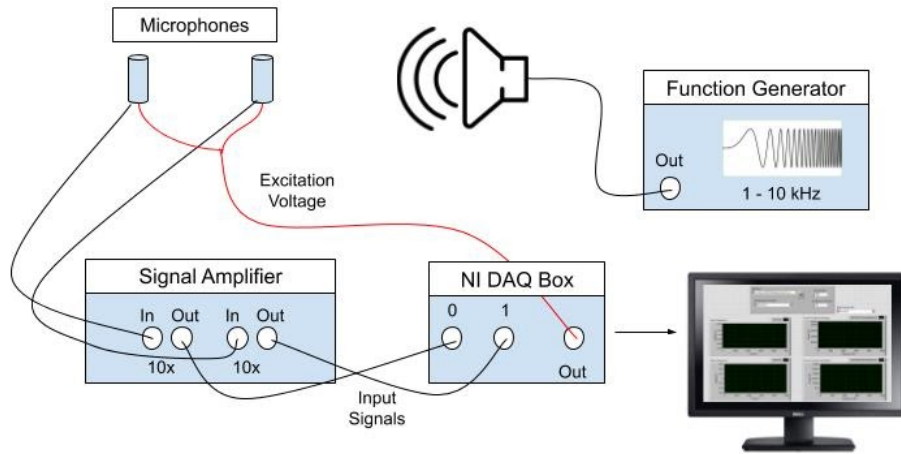


Figure D2: Electrical Schematic of Frequency Sweep Experiment. Uses a Function Generator to Produce the Signal which is Read by the NI DAQ Box and Monitored Through LabVIEW

Appendix E: Porosity Calculations

The volume of air in an average pore in an earplug was calculated as follows:

1. Using the exported data from a horizontal cross-section image, identify the X_1 and X_2 values of each pore in the analyzed profile.
 - a. X_1 is the x value that corresponds to the start of a pore.
 - b. X_2 is the x value that corresponds to the end of a pore.
 - c. These values can be identified by looking at the corresponding y-values.
 - d. When the y-values hit a local maximum, mark that as the beginning of a pore.
 - e. When the y-values hit a local minimum, mark that as the middle of a pore and its lowest point.
 - f. When the y-values return to a local maximum, mark that as the end of the pore.
2. To find the diameter of a pore, subtract X_1 from X_2 and multiply this value by the “pixilation factor” (PF).
 - a. The pixilation factor is the correction factor that converts the exported “x-values” of the data into units of micrometers as opposed to pixels.

$$a = (X_2 - X_1) * P. \tag{E1}$$

3. Complete repeat these steps for all the pores in the cross-section. Average these values and this will be the “a” value when finding the average volume of a pore.
4. Repeat steps 1-3 for the vertical cross-section image.
5. This value will be the “b” value when finding the average volume of a pore.

$$b = (X_2 - X_1) * PF. \tag{E2}$$

6. Complete the following steps for both the horizontal and vertical cross-section images:
 - a. Identify the Y-value that corresponds to X_1 .
 - b. Identify the Y-value (Y_3) that corresponds to the local minimum found earlier. These values are already in micrometers.
 - c. Subtract Y_3 from Y_1 .
 - d. This will result in the approximate depth of the pore.
 - e. Find the approximate depth for every pore in the image.
 - f. Average all of the depth values from both images. The resulting value will be the “c” value when finding the average volume of a pore.
7. Plug in the “a”, “b”, and “c” values to the equation for the volume of an ellipsoid.

$$V = \frac{4}{3} * \pi * a * b * c. \tag{E3}$$

8. This value is the volume of the average pore in the earplug sample.
9. Complete these steps for every porous earplug sample.

Using the value of the average volume of air in an earplug pore, the volume of air in the entire plug was calculated as follows:

1. Estimate the volume of the entire plug by utilizing the equation of a cylinder.

$$V = \pi * r^2 * h. \tag{E4}$$

2. Estimate the total number of pores in the sample.
 - a. Start by counting the number of pores that can be seen in the image taken by the microscope.
 - i. This step can also be completed by completing an edge detection image analysis using MATLAB software.
 - b. Estimate the volume of this image by using the given x and y values (given in pixels) of the screen and convert this to micrometers by multiplying by the pixilation factor discussed above.
 - c. Use the average depth of a pore for the third value needed to calculate the volume.

$$V_{\text{screen}} = x_{\text{screen}} * y_{\text{screen}} * z_{\text{depth}}. \tag{E5}$$

- d. Divide the total volume of the plug by the volume of this individual screen.
 - e. This value is the number of “screens” in the entire plug.
 - f. Multiply the number of pores in one screen by the total number of screens in the entire plug.
 - g. This is the number of pores in the entire earplug.
3. Multiply the number of pores in the plug by the average volume of a single pore.
 - a. This value will be the total amount of air in the entire plug.
4. To find the percent volume of air in each plug, divide the volume of air by the volume of the entire plug and multiply this value by 100.

A range for the volume of air was calculated by completing the same steps as above but substituting the volume of the entire plug with the Equation E6. This equation simulates the volume of a compressed earplug.

$$V = \pi * r_1^2 * h_1^2 + \pi * r_2^2 * h_2^2. \tag{E6}$$

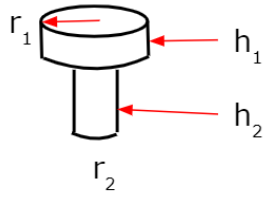


Figure E1: Estimation of the Volume of Compressed Earplug

Appendix F: Microscopy Results for Various Sample Cross-Sections

A cross section of sample 2 is shown in Fig. F1. Shown at 100x magnification the sample is seen to have a fairly uniform pore size of around 200 – 300 [um]. The topographical map shows a maximum depth range of nearly 500 [um] with most pores extending approximately 200 [um].

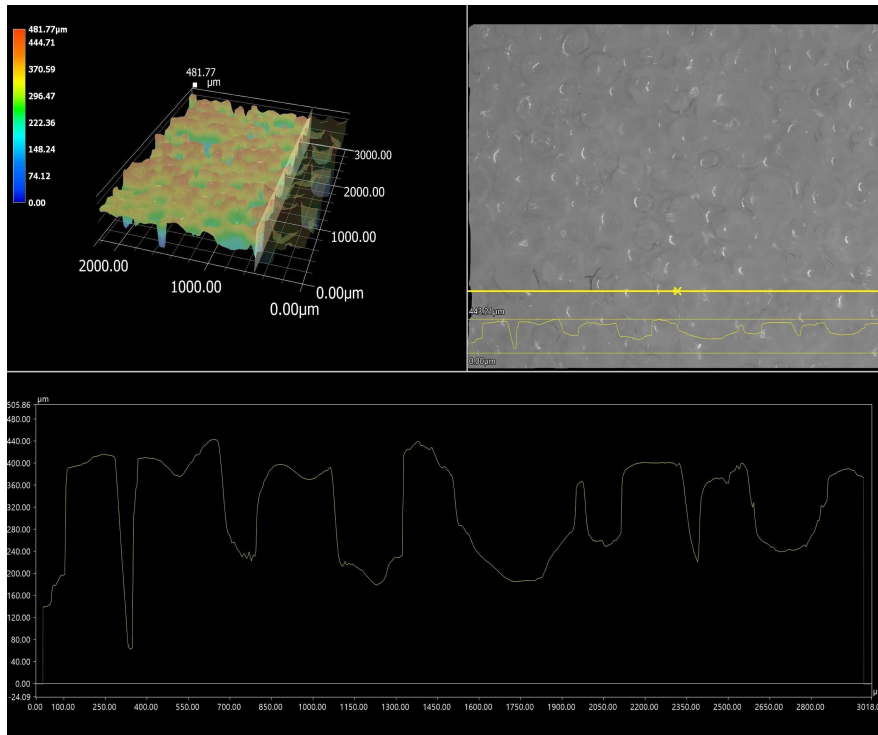


Figure F1: Sample 2 (Manufacturing) Microscope Imaging

The 3M earplugs, seen in Fig. F2, have pores that can be clearly seen without magnification. An investigation at 100x shows that the pore size is very variable with large pores around 300 – 400 [um] and smaller pores measuring 150 [um]. While the extreme depth is nearly 600 [um], the average depth is again around 200 [um].

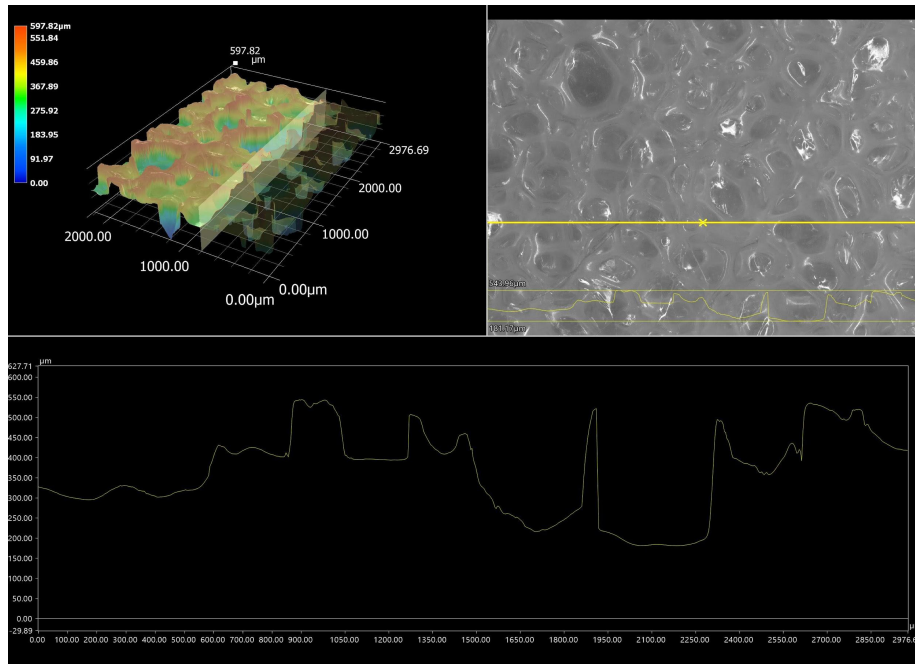


Figure F2: Sample 3 (3M) Microscope Imaging

Fig. F3 shows a cross section of the triple flange earplugs. At 100x the pores are still impossible to distinguish, and the material seems homogenous. Parabolic stress lines that can be seen are likely a result of the method of cutting.

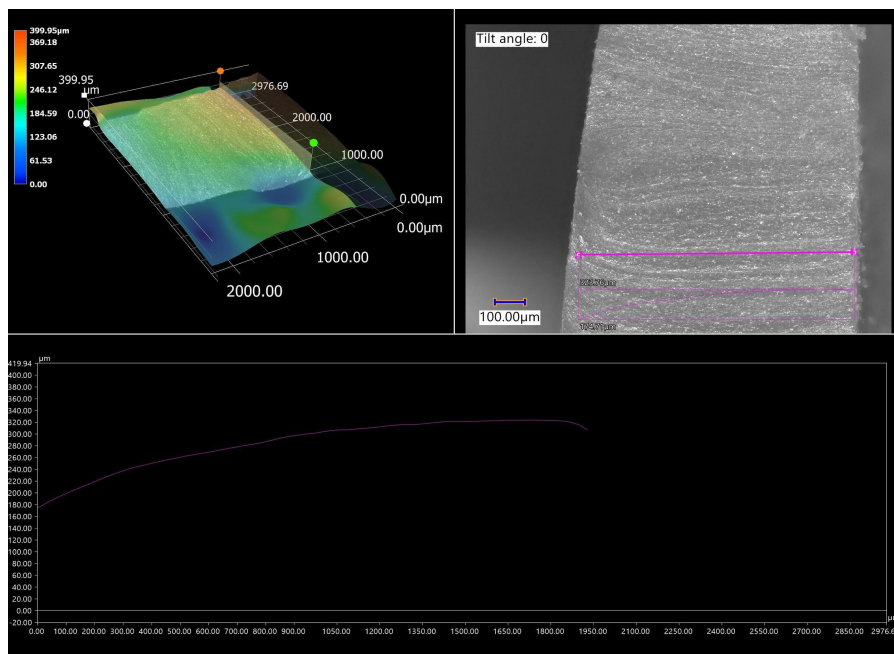


Figure F3: Sample 4 (Triple Flange) Microscope Imaging

As expected, a study of the wax earplugs, Fig. F4, shows a similar results as the triple flange plugs. Pores are again indistinguishable under 100x magnification and the same stress lines appear, again from the method of cutting our material.

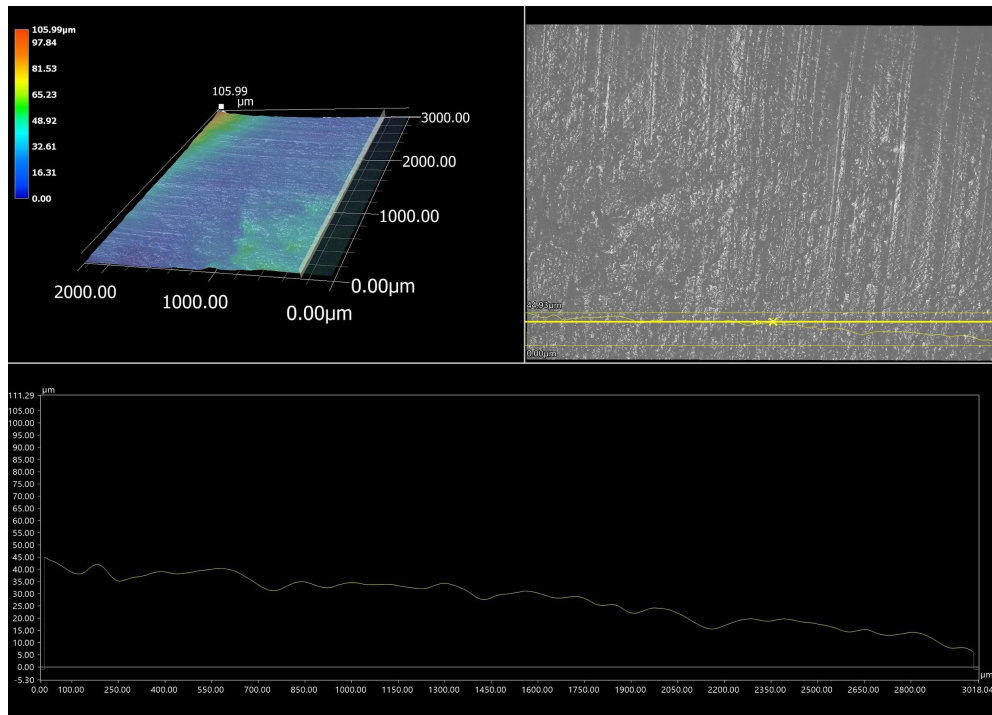


Figure F4: Sample 5 (Wax) Microscope Imaging

Appendix G: Detailed Computational Setup

Porous Earplug Boundary Conditions:

The portion of the model that defines the earplug is created in the poroelastic waves domain. This geometry is shown in Fig. G1 as the front 2 cm of the cylinder. The poroelastic waves module was utilized for its ability to homogenize a porous medium and the added input parameter such as porosity in material properties. Through this module, various solid materials along with fluid matrix materials can be applied.

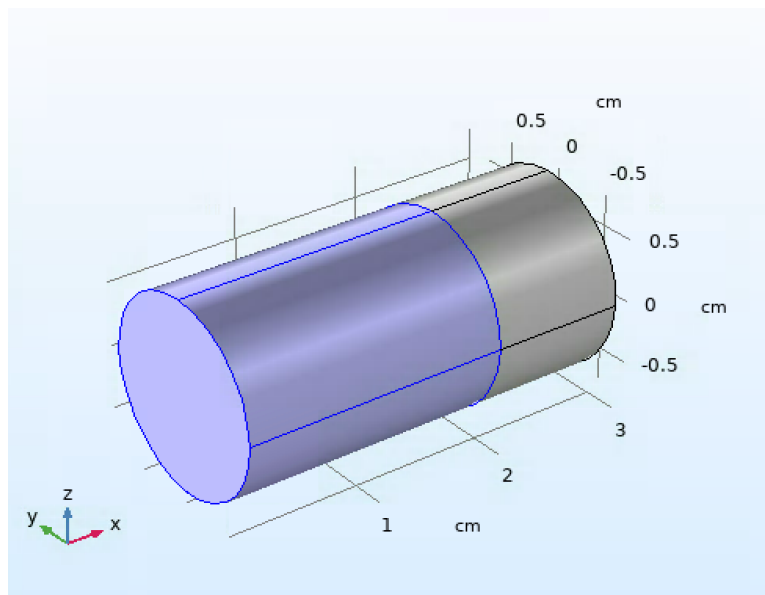


Figure G1: Portion of Model Described by Poroelastic Waves Domain (Shown in Blue)

The earplug is rigidly constrained on all sides shown in blue in Fig. G2. This means there are no displacements or rotations along the boundary edges. We made this simplification because our study was primarily focused on material performance and not material-ear canal interaction.

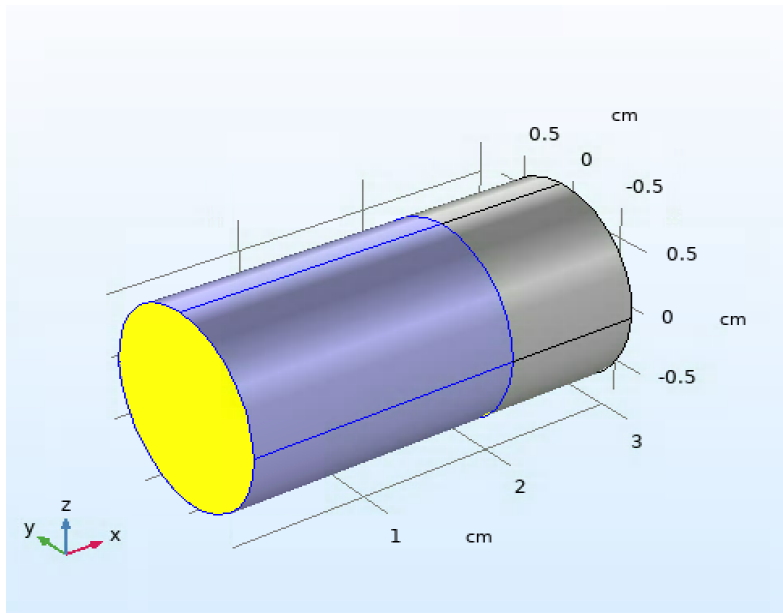


Figure G2: Fixed Boundaries (Shown in Blue)

The pressure was applied as a uniform input on the surface shown in blue in Fig. G3. We used an input of 1 Pa as this was consistent with the experimental stimulus.

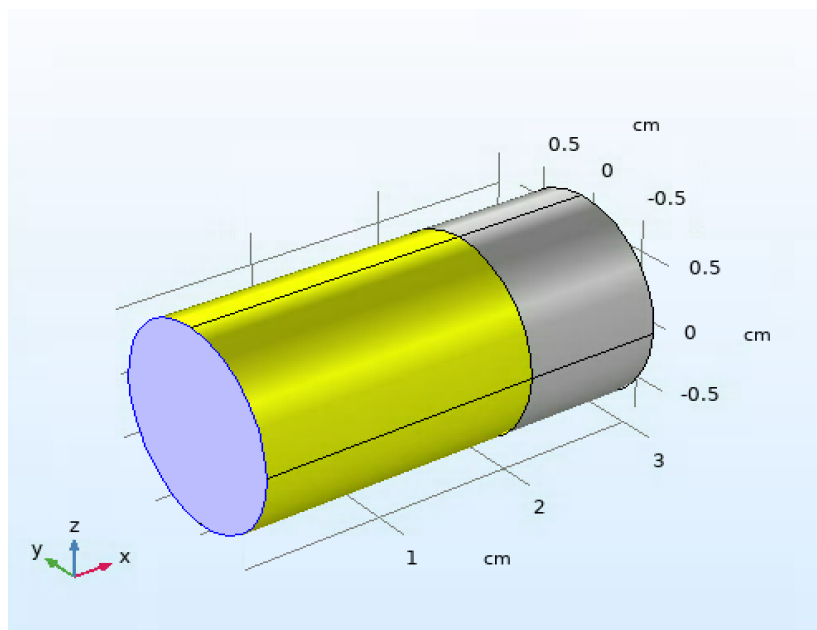


Figure G3: Porous Input Pressure 1Pa (Shown in Blue)

The back 1 cm of the model, shown in Fig. G4, represents the occluded air between the plug and the ear drum. The pressure acoustics domain is used as this is a single material domain.

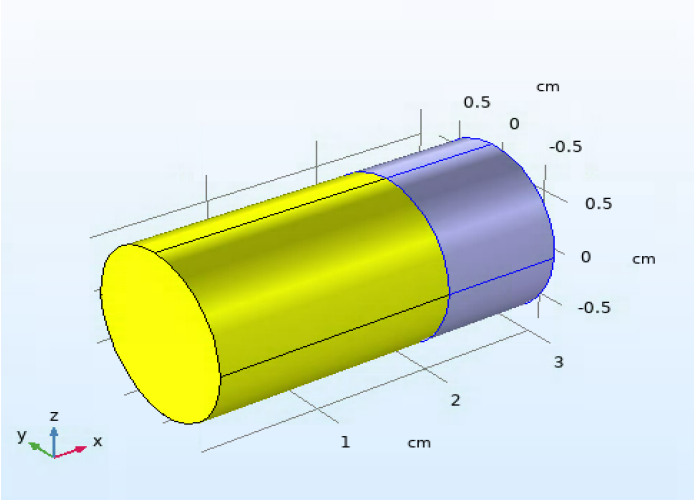


Figure G4: Portion of Model Described by Pressure Acoustics, Frequency Domain (Shown in Blue)

Triple Flange Earplug Boundary Conditions:

The triple flange earplug geometry was imported into the COMSOL environment and a channel of air, shown in Fig. G5, was created to surround it. Since the triple flange earplug has a tapered geometry, the ear canal was modeled here as a cylindrical cone so air would not pass over the flanges.

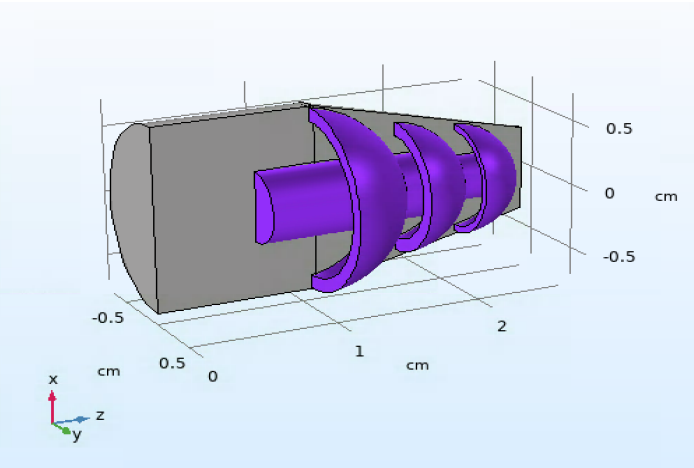


Figure G5: 3D Reference Geometry of Triple Flange Plug and Ear Canal

The 3D geometry shown in Fig. G5 was then converted to the axisymmetric 2D model in Fig. G6. This was valid because of geometric symmetries and applied to reduce computational analysis time.

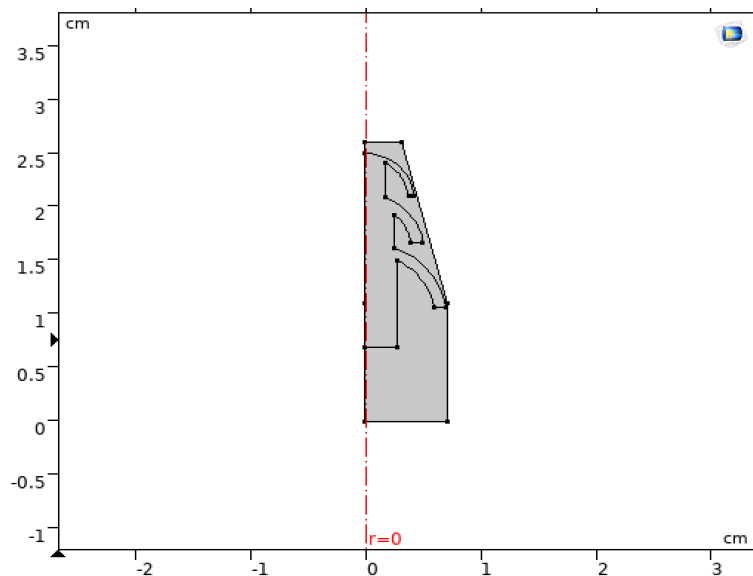


Figure G6: 2D Axisymmetric Simplification of 3D Geometry

The entire triple flange model was built entirely in the pressure acoustics domain, shown in blue in Fig. G7. The poroelastic waves module was not needed as the triple flange plug is made from a uniform silicone material.

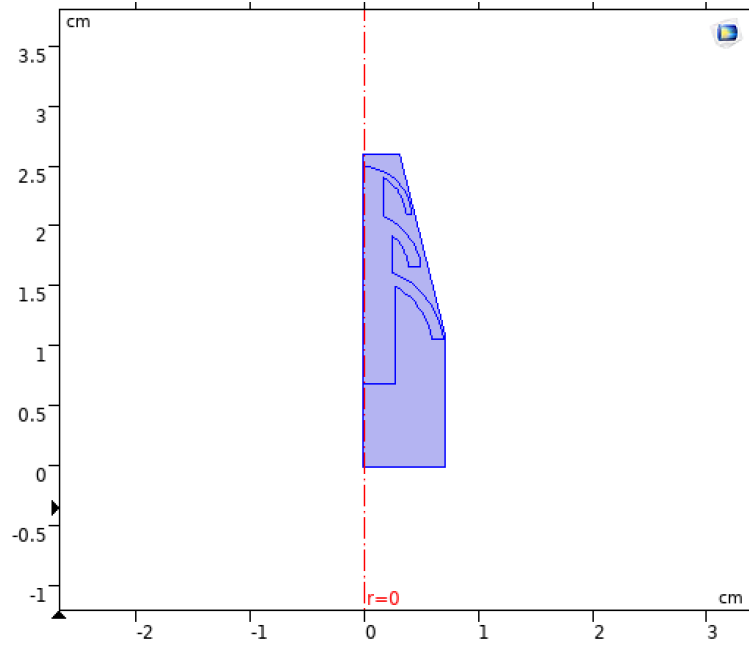


Figure G7: Portion Modeled in Pressure Acoustics, Frequency Domain (Shown in Blue)

The blue line at $r = 0$ in Fig. G8 shows the axis of symmetry with which the model results can be rotated to create a 3D representation.

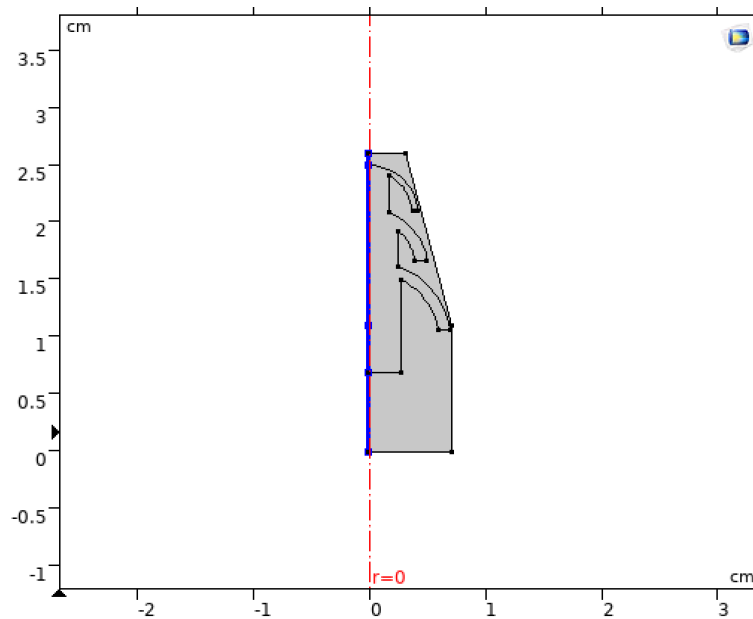


Figure G8: Axis of Symmetry for 2D Geometry (Central Blue Line)

Fig. G9 shows the outer walls of the ear canal are modeled as sound hard boundaries. This means that pressure is primarily reflected from these walls and not absorbed.

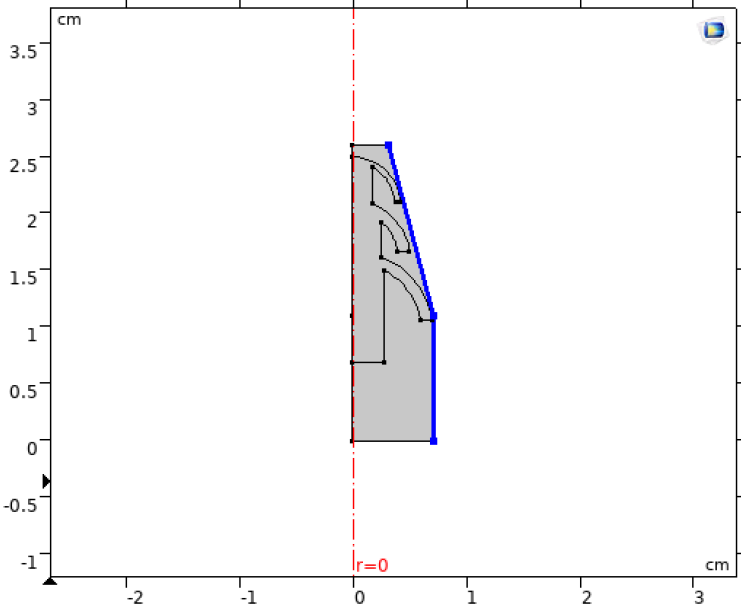


Figure G9: Sound Hard Boundary Walls (Blue Lines)

The input pressure is applied as 1 Pa, the blue line in Fig. G10.

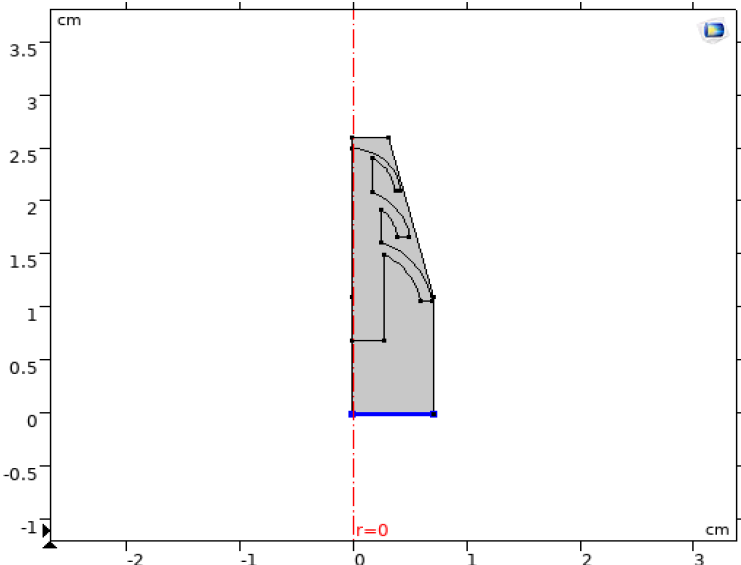


Figure G10: Input Pressure 1Pa (Blue Line)

To accurately measure the output, the eardrum is modeled as a sound soft boundary, the blue line in Fig. G11. This means that pressure is absorbed and not re-reflected into the ear canal, so an accurate measure of the pressure gradient can be visualized.

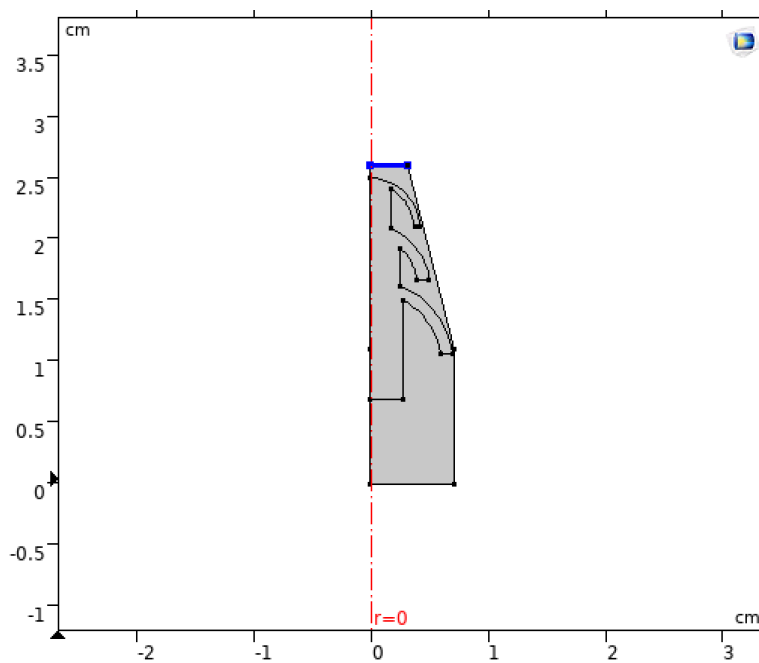


Figure G11: Sound Soft Exit Boundary (Blue Line)

Appendix H: Instructions to Develop Computational Model

The instructions to develop the porous computational model are described in this section. Modifying this for the triple flange model will be described at the end. The model was created off of a sample model in COMSOL called: Absorptive Muffler.

The description of how to set-up the Absorptive Muffler model can be found at:

https://www.comsol.com/model/download/624411/models.aco.absorptive_muffler.pdf

A COMSOL tutorial video explaining the Absorptive Muffler model can be found at:

<https://www.comsol.com/video/introduction-to-modeling-acoustic-structure-interaction-with-comsol-aug-2-2018>

After opening the Absorptive Muffler example file, follow the above link to the tutorial video. This will show you how to input the poroelastic waves domain – the only remaining step will be updating geometry to your desired geometry. The below tutorial builds the model from scratch. Use these in conjunction to fully understand the set-up.

Building Model in Fig. H1 from Scratch:

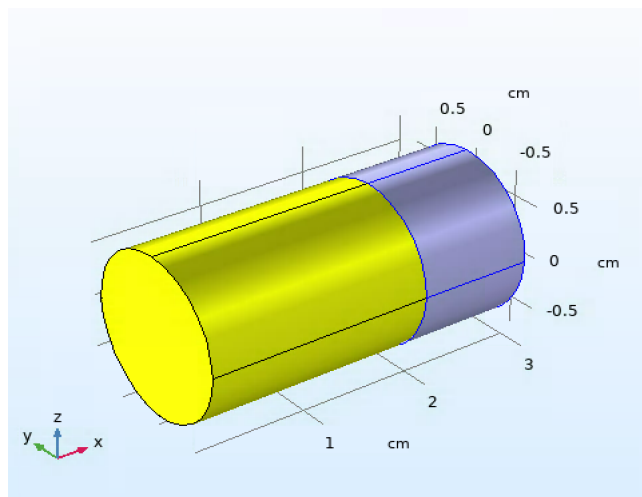


Figure H1: Porous Earplug Model to be Built

Creating environment:

- 1) Create a new COMSOL project

- 2) Select Model Wizard, then 3D
- 3) Search for Pressure Acoustics, Frequency Domain – select and click add
- 4) Search for Poroelastic Waves – select and click add
- 5) Click Study and then Done

Creating Geometry:

- 6) In the model builder click geometry, change units to cm
- 7) Creating Earplug Geometry
 - a. Under the Geometry tab, click Cylinder
 - b. Input desired radius and length (.75 cm and 2 cm in our case)
- 8) Creating Occluded Air
 - a. Follow the same procedure as in 7, note that you need to input an offset of 2cm in the correct direction

Selecting Physics Domains:

- 9) Click on the Poroelastic Waves tab, click on the number corresponding to the air geometry (likely 2) and deselect using the – symbol
- 10) Click on the Pressure Acoustics tab, click on the number corresponding to the earplug geometry (likely 1) and deselect using the – symbol

Setting Boundary Conditions:

- 11) Right click on the Poroelastic Waves tab and select fixed constraint, select the four sides of the earplug
- 12) Right click on the Poroelastic Waves tab and select porous pressure, select the external face of the earplug and input desired pressure
- 13) Right click on the Pressure Acoustics tab and select port, select the external face of the volume of air
- 14) For the volume of air, you can experiment with having sound hard and sound soft boundaries as the side boundaries
- 15) Look through the different boundary options to understand what is available. Think about what you are trying to model and what boundaries are most accurate.

Inputting material:

- 16) A material will need to be applied to both domains, and two materials will be selected for the porous medium

- 17) Click the materials tab and explore options, double click air to add it to possible model materials
- 18) Search for the solid earplug material and double click to add it to possible model materials (we primarily used polyurethane)
- 19) Follow this process again if the fluid matrix is not air
- 20) Select the material tab in the model builder
- 21) Click air, make sure that only the air domain is selected
- 22) In the Poroelastic Waves module, select the Poroelastic Material dropdown
- 23) Change model type to Biot-Allard
- 24) Change the Porous Elastic material to the desired solid matrix material
- 25) Change fluid material to desired fluid matrix material
- 26) Input desired material properties (these can be accessed under materials in the model builder. Note that materials used in Poroelastic domain will have additional input parameters)

Creating Multiphysics Coupling:

- 27) Right click on the Multiphysics tab, select Acoustic-Porous boundary
- 28) In the Graphics window, click on the select box button
- 29) Draw a box around the whole model, the boundary between the plug and air should be the only thing selected

Running the Experiment:

- 30) Click the study tab, select add study
- 31) Select the desired type of study (most likely Frequency Domain)
- 32) A study will be added to the Model Builder, here you can change frequency range
- 33) Right click on Study 1, select parametric sweep (this will allow for a sweep of one or multiple parameter values. To do this, create a parameter under global definitions, change the material property to that variable and input the desired range in the parametric study)
- 34) Run the experiment! Play around with different ways to visualize results such as cut planes which show cross sections, cut points which show values at a specific point, and 3D models.

Developing Triple Flange Model:

While the triple flange geometry is more complicated, the model is in a way simplified as it only uses one physics domain (Pressure Acoustics). To set up the model, import the triple

flange geometry (most easily built in SolidWorks). Creating the ear canal around this imported geometry is very similar to creating geometry in the porous earplug model. We utilized the 2D axisymmetric simplification which greatly reduces computational time, the tutorial to transfer from the 3D model to 2D axisymmetric can be found at the below link.

Creating 2D Axisymmetric Model from 3D Model:

<https://www.comsol.com/video/creating-2d-models-from-3d-geometries-in-comsol-multiphysics>

Appendix I: LabVIEW Code for Shock Tube

The previous MQP team developed a LabVIEW Code that included four pressure sensors. There was one in the driving section of the shock tube, two within the driven section of the shock tube, and one external pressure sensor. In order to be able to properly measure the attenuation level, there needed to be a pressure sensor before and after the earplug sample similar to the setup of the microphones in the Frequency Sweep Experiment. We updated the LabVIEW Code developed by the previous team to include an additional pressure sensor and controls to convert the Voltage/Time data to pressure to match the units of the other sensors.

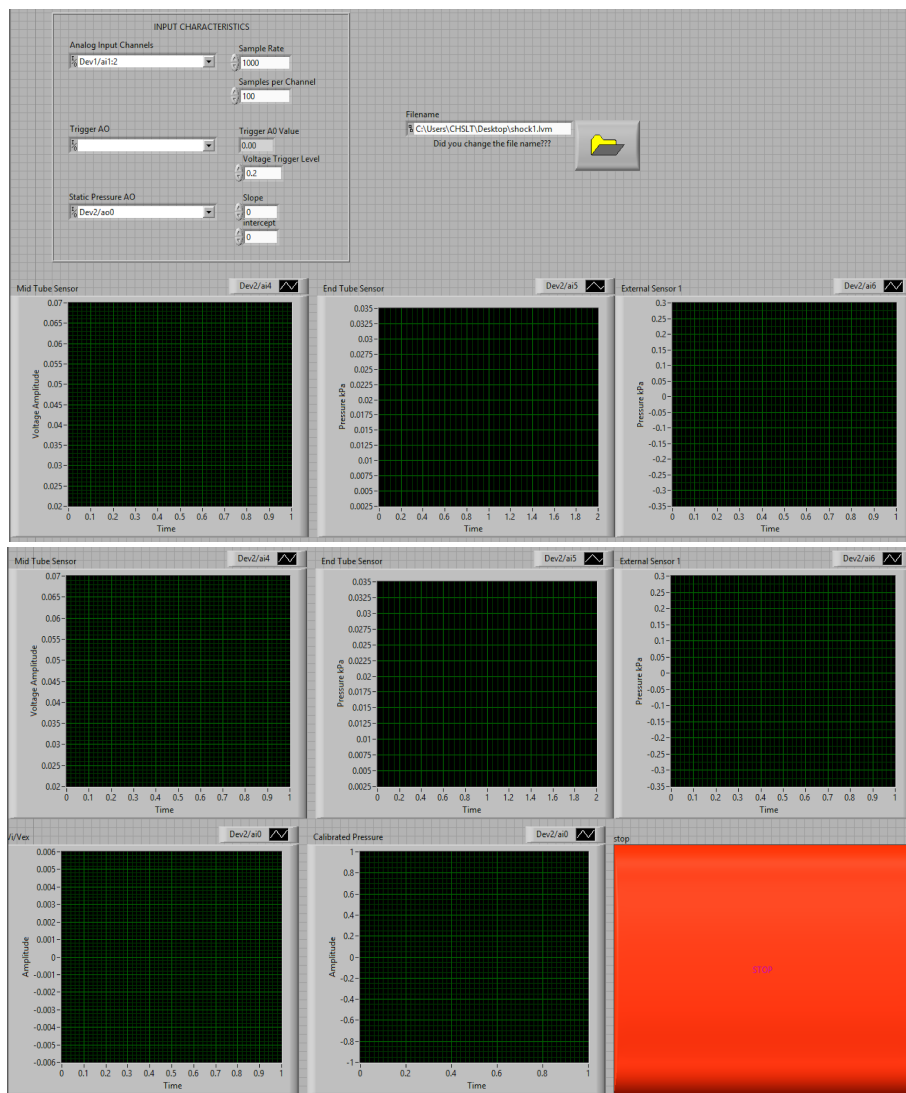


Figure 11: Front Panel for Shock Tube Code

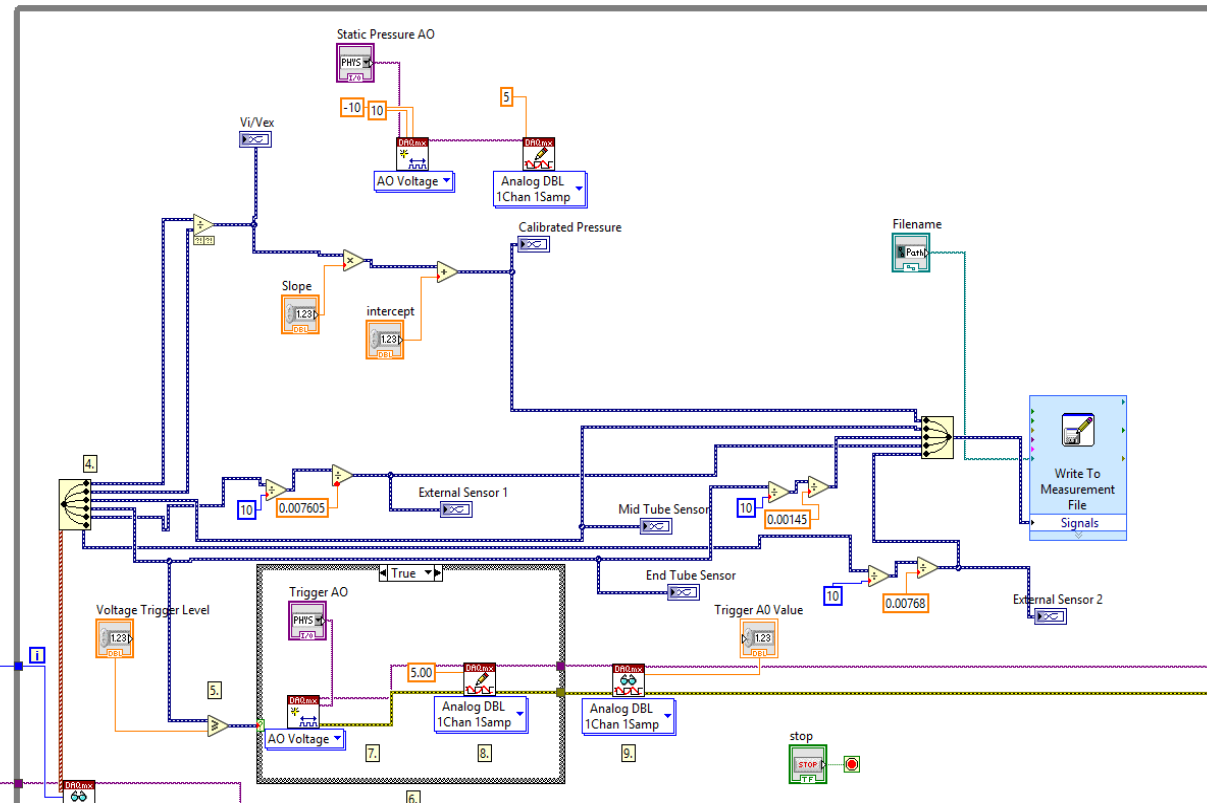


Figure 12: Overall Block Diagram for Shock Tube Code

The change that we made to accommodate the additional sensor can be seen in Fig. 13.

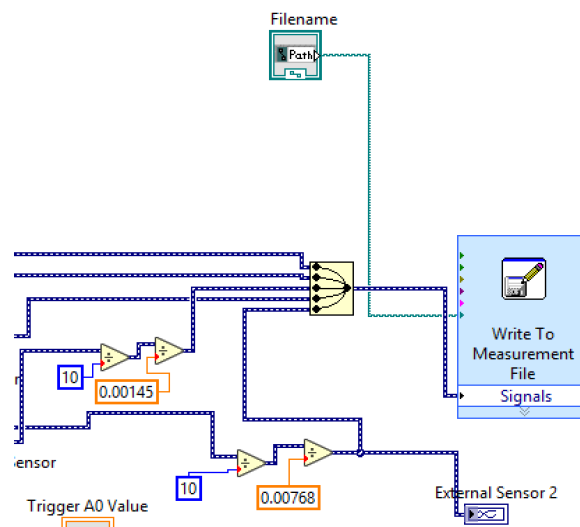


Figure 13: External Sensor with Conversion